Collisional line broadening and mixing in the Raman spectrum of CO perturbed by N2: Experimental measurements and theoretical calculations

D. Paredes-Roibás, R.Z. Martínez, H. Jóźwiak, Franck Thibault

Collisional line broadening and mixing in the Raman spectrum of CO perturbed by N_2: experimental measurements and theoretical calculations

Denís Paredes-Roibás [a,b], Raúl Z. Martínez [a], Hubert Jóźwiak [c], Franck Thibault [d]

[a] *Instituto de Estructura de la Materia, IEM-CSIC. Serrano 123, 28006 Madrid, Spain.*
[b] *Departamento de Ciencias y Técnicas Fisicoquímicas, Facultad de Ciencias, Universidad Nacional de Educación a Distancia (UNED), Paseo de la Senda del Rey 9, E-28040 Madrid, Spain.*
[c] *Institute of Physics, Faculty of Physics, Astronomy and Informatics, Nicolaus Copernicus University, Grudziadzka 5, 87-100 Toruń, Poland*
[d] *Univ Rennes, CNRS, IPR (Institut de Physique de Rennes)-UMR 6251, F-35000 Rennes, France*

Abstract

We present a joint experimental and theoretical study of line broadening and mixing in the Q branch of the Raman spectrum of CO perturbed by N_2 at 77, 195 and 298 K. Advanced methods and facilities have been used for both aspects of the study: the experiments were conducted using a high-resolution stimulated Raman spectroscopy setup, while the calculations were performed using a quantum dynamical formalism and one of the most recent potential energy surfaces available. Line broadening coefficients were determined experimentally for rovibrational lines up to $j = 11$ at 77 K, $j = 15$ at 195 K and $j = 19$ at 298 K, and calculated for lines up to $j = 6$ at the three temperatures. Line mixing was also observed and coefficients measured for lines up to $j = 8$ at 77 K and $j = 5$ at 195 K, and again calculated up to $j = 6$ at the three temperatures. A comparison shows an overall very good agreement between experiments and calculations for both sets of coefficients. Additional calculated data for the pure rotational R and S lines are also provided.

Email address: denis.paredes@iem.cfmac.csic.es (Denís Paredes-Roibás)

Preprint submitted to Journal of Quantitative Spectroscopy and Radiative Transfer August 2, 2021

Graphical Abstract

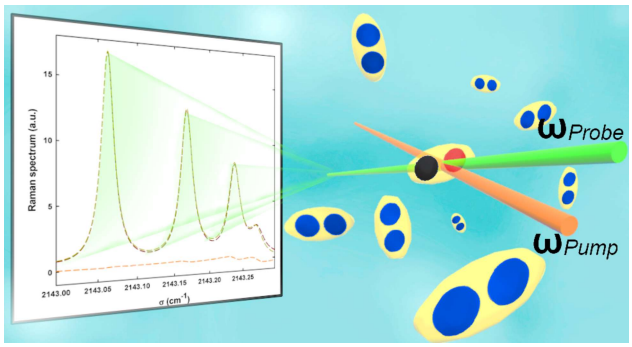

Keywords:
Collisional Broadening, Line Mixing, Stimulated Raman Spectroscopy, Quantum Dynamical Calculations, CO-N_2

1. Introduction

The CO-N_2 collisional system has been the object of numerous studies in the last decades. One of the attractions of the system lies in the possible formation of the CO-N_2 dimer and the study of its rovibrational energy levels, a topic that has seen a renewed interest in the last 10 years [1–4]. However, most of the attention this collisional system has received stems from its presence in a number of different environments and from the information that studies of its spectral features can provide about them. The closest of these environments is the Earth's atmosphere, mainly constituted by N_2 but with a trace presence of CO. The role of CO in different atmospheric processes like the CO-OH-CH_4 cycle [5, 6], one of the self-cleansing processes of the troposphere, coupled with the fact that part of this atmospheric CO originates from anthropogenic emissions [5], has attracted considerable interest.

Besides Earth, the presence of CO has been reported also in some bodies of our solar system with weak atmospheres that are covered by different ices. The sublimation of these ices produces atmospheres in which both CO and N_2 are present. This is the case of Pluto [7], Titan [8] and Triton [9], in which significant amounts of both molecules have been found by infrared spectroscopy. Furthermore, in exoplanetary atmospheres such as those of HD 209458b [10], HD 189733b [11] and WASP-12b [12], among other exoplanets [13], CO has also been detected. The possibility that CO plays a role in the

formation of planetary hazes in these types of atmosphere has been explored [14].

Given that most of the measurements used for the remote determination of concentrations of molecular species, be it in the Earth's atmosphere, an exoplanetary atmosphere or an interstellar cloud, are obtained by spectroscopic means, both ground- and satellite-based, and that the shape of molecular spectra strongly depends on temperature and pressure changes, it is critical to have accurate knowledge of the pressure broadening and shift coefficients of the species under study at different temperatures for a successful extraction of the information contained in these spectra.

Other than atmospheric and astrophysical studies, there is also a number of technological applications in which the CO-N_2 system is involved. The most important one is probably combustion studies: the technique of coherent anti-Stokes Raman spectroscopy (CARS) is widely used for temperature measurement in combustion environments, usually through monitorization of the CARS spectrum of N_2 [15, 16], but also for the determination of the concentration of species like CO [16], which often appear as minor combustion products. CARS has been used to determine temperatures and products concentration through monitorization of CO and N_2 spectra in combustion engines [17], diagnosis of solid propelants [18] or jet diffusions flames [19] among other combustion applications. Again, a good knowledge of the spectra of these molecules at different temperatures and pressures is key for the interpretation of the experimental data.

Due to the weak dipole moment of the CO molecule, the CO-N_2 collisional system can be studied using infrared (IR) spectroscopy. This is reflected in the large number of studies, both experimental and theoretical, performed on the P and R branches of the fundamental vibration of CO perturbed by N_2 carried out in the last decades. In particular, Nakazawa et al. [20, 21] studied the R branch of CO self-perturbed and perturbed by N_2 at several temperatures. Drascher et al. [22] measured the collisional broadenings and shifts of R-branch lines perturbed by Ar, N_2, O_2 and H_2. Predoi-Cross et al. [23] studied the broadening and shifiting of lines in the P and R branches of the rovibrational spectrum of CO perturbed by N_2 at 348 K. Besides the fundamental vibrational band, broadenings, shifts and asymmetries have also been measured in other IR-active bands like the v= 0 $\rightarrow$ 2 [24] and v= 0 $\rightarrow$ 3 [25] overtones. There are also a number of other works on specific pure rotational transitions such as $j = 0 \rightarrow 1$ [26–29], $j = 1 \rightarrow 2$ [29, 30], $j = 2 \rightarrow 3$ [29, 31], $j = 3 \rightarrow 4$ [29], and $j = 4 \rightarrow 5$ [32, 33].

The only *ab initio* determination of CO linewidth parameters up to today was performed recently by Jóźwiak et al. [34] for the pure rotational R(0) line. The dynamical calculations to this end were performed on three recent potential energy surfaces (PES) for the CO-N_2 interacting pair [2–4]. We refer the reader to the numerous studies devoted to the R lines of CO perturbed by N_2 listed in Ref. [34].

Compared to the number of IR studies, experimental studies of CO perturbed by N_2 by means of Raman spectroscopy are scarce in the bibliography, and nearly all of them focus on pure rotational transitions. Afzelius et al. [35] obtained rotational CARS spectra in CO-N_2 mixtures in order to compare the experimental linewidths with the ones predicted by their model. More recently, collisional line broadening measurements on the pure rotational S branch of the Raman spectrum of CO perturbed by N_2 were performed by Hsu et al. [36]. An experimental study closer to the one presented in this article was conducted years ago by Roblin et al. [37]. CARS was used to record the Q branch of the fundamental vibration of CO perturbed by N_2. The experiment, however, was performed at pressures between 1 and 100 atm, a much higher regime than the one explored in the present work, and the authors did not attempt to obtain experimental broadening or mixing coefficients.

Theoretical studies of line broadening and mixing coefficients for rovibrational Raman lines in this collisional system are also scarce. In the work of Roblin *et al.* [37], the transfer of intensity between lines due to line mixing was modeled via the semi-empirical modified energy gap law, the parameters of which were adjusted on the linewidths derived from the semi-classical method of Robert-Bonamy. The most recent calculation of Raman line broadening coefficients to date was performed by Afzelius et al. [38]. Using the Robert-Bonamy formalism, the authors calculated line broadening coefficients for the isotropic Raman Q branch lines of the fundamental vibration of CO perturbed by N_2, as well as for infrared R lines.

This work presents a study, both experimental and theoretical, of line broadening and mixing in the Raman spectrum of the fundamental vibrational band of CO perturbed by N_2 at 77, 195 and 298 K. Collisional line broadening and line mixing coefficients for the rovibrational lines in the Q branch of the band have been obtained by means of high resolution Raman spectrocopy and quantum dynamical calculations at three different temperatures. Both approaches are described in detail in the following sections.

2. Experimental part

2.1. Methods

The spectral line profiles analyzed in this work belong to rovibrational lines of the Q branch ($\Delta j = 0$) in the Raman spectrum of the fundamental vibration (v= 0 →v= 1) of the molecule of CO perturbed by collisions with N_2. The high resolution Raman spectra required for these analyses were obtained by means of an experimental setup based on the technique of stimulated Raman spectroscopy (SRS). SRS was initially demonstrated by Owyoung with continuous (cw) laser sources [39], but the relatively low sensitivity of the technique led to the development of the quasi-continous (quasi-cw) scheme in which one cw and one pulsed laser source are used [40, 41]. Our setup follows this quasi-cw scheme. Through the years, different variations of the experimental setup have been used in our laboratory to obtain high resolution Raman spectra of rovibrational and pure rotational transitions for frequency [42], line profile [43] and even collisional energy transfer [44] studies. For the present work we set up a configuration similar to the one described in [45], with a number of relevant differences and modifications that are described in detail in the following paragraphs. An updated schematic layout of our setup is depicted in Fig. 1.

The cw probe beam is generated by a single-mode Ar^+ ion laser (Spectra-Physics 2080) tuned to the 529 nm emission line. The laser is frequency-stabilized and actively locked to a molecular reference, a hyperfine component of the electronic absorption spectrum of $^{130}Te_2$ in the vapor phase. The transition at 18909.44611 cm^{-1}, measured in our laboratory [46], has been used as reference throughout this work. The system is able to reach a linewidth, determined by the residual jitter, lower than 500 kHz (1.7×10^{-5} cm^{-1}). The output power of the laser is set to $\sim$ 500 mW.

The pump beam is obtained by pulsed optical amplification of a cw tunable seed generated by a single-mode cw ring dye laser (Sirah Mattisse DS), operated with a solution of Rhodamine 6G for this experiment. A three-stage pulsed dye amplifier (Quanta-Ray PDA-1) with a solution of Kiton Red and pumped by the second harmonic of a 10 Hz Nd:YAG laser is used for the optical amplification of the cw seed. The resulting tunable pulses have near-Gaussian temporal and spectral shapes with $\sim$ 12 ns of temporal full width at half maximum (FWHM) and $\sim$ 70 MHz of spectral FWHM. Pulse energies of several tens of mJ can be reached.

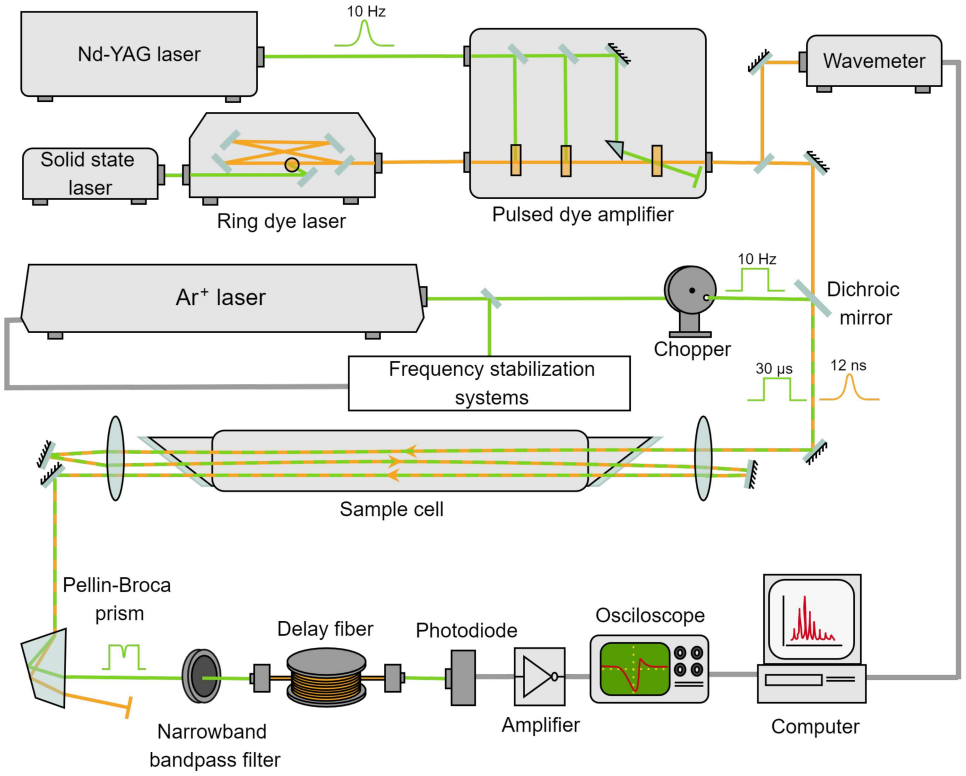

Figure 1: Schematic experimental setup of the stimulated Raman loss experiment. For the sake of simplicity some of the elements mentioned in the text have been omitted.

Raman frequencies are obtained at any point by simple substraction of the frequencies of the probe and pump beams. The frequency of the locked probe beam is well known and kept constant throughout the experiment, while the frequency of the tunable pump beam needs to be measured at every point (pulse). This task is performed by a high accuracy wavemeter (HighFinesse WSU-10), which provides a nominal accuracy of 10 MHz (3σ) and is periodically calibrated using as a reference radiation a fraction of the frequency-locked probe beam.

Two different sample cells were used for this work, one made of Pyrex glass and the other one of stainless steel, in order to reach the various sample temperatures at which spectra were recorded. The Pyrex cell, consisting of a central cylindrical sample chamber and surrounding coolant and isolation chambers, has already been described in prior works [45, 47]. In the present

one it was used for the obtention of the 77 K spectra, with liquid nitrogen as coolant, and of the 298 K spectra. The stainless steel cell follows a similar design philosophy: an inner sample chamber of cylindrical shape with a length of ∼90 cm, an internal diameter of 2.5 cm and ultraviolet fused silica (UVFS) windows installed on both ends at Brewster's angle. The central part of this cylinder, up to a few centimeters from each end, is enclosed by a second, cuboidal-shaped stainless steel structure with its top face open (i.e. a stainless steel "box"). This box acts as a container for the coolant and allows the central body of the cell to be submerged in it. The outside of the box is insulated with a layer of styrofoam. This cell was used for the obtenton of the 195 K spectra with dry ice as coolant.

Prior to its arrival to the sample cell, the probe beam goes through an electromechanical modulator ("chopper") synchronized with the Nd:YAG laser clock to produce square "pulses" of 30 μs width at a repetition rate of 10 Hz to avoid saturation of the detection photodiode. The probe and pump beams, both vertically polarized, are spatially overlapped by means of a dichroic mirror, focused into the sample cell by an f=500 mm lens and recollimated by a similar lens after the cell. A triple pass is used to increase the sensitivity of the experiment. After this, the two beams are separated using two Pellin-Broca prisms. The pump beam is dumped, while the probe beam passes through a narrowband bandpass filter (Semrock MaxLine LL01-532-12.5) to block any residual pump light and is injected into a 100 m long multimode fiber. The role of the fiber is to introduce a delay of $\sim$ 400 ns in the detection of the Raman signal being carried by the probe beam, so that this detection and measurement stage is not affected by the electrical noise associated to the Q-switch electronics of the Nd:YAG laser. At the output of the fiber, the probe radiation is refocused on the surface of a fast PIN photodiode (EG&G FND-100). The electrical output of this photodiode passes through a high-pass filter that removes the DC components and is fed to a transimpedance amplifier (FEMTO HCA-400M-5K-C), whose output is sent to a digital oscilloscope (Tektronix DPO7254) operating in Fast Frame (hardware-driven) mode. The oscilloscope, triggered synchronously by the Nd:YAG laser clock, digitizes and stores all the traces. Each one of these traces contains information about variations in the intensity of the probe laser in the temporal window corresponding to its interaction with a pump laser pulse inside the sample cell. Analyses of these data are performed in a separate computer with code specifically developed by us using the Matlab package, which carries out the necessary numerical integration of the traces

as well as additional noise filtering, frequency assignment to each data point and other postprocessing tasks to produce the final Raman spectrum.

CO and N_2 were provided by Air Liquide with purities >99.997% and >99.999% respectively. Prior to the obtention of CO-N_2 Raman spectra, several preparation runs were conducted with samples of pure CO at low pressures (2 to 8 mbar) and at the three temperatures of interest. These runs accomplished two main objectives:

- The determination of the Gaussian contribution present in the line profiles at each one of these temperatures. To this end, the experimental lines were fitted with Voigt profiles, and the results confirmed a minimal Lorentzian contribution, as expected at these pressures, and a dominant Gaussian contribution. This Gaussian contribution results from the convolution of the Doppler profile and the apparatus function, both of which are also Gaussian. Since the Doppler contribution for any line at a given temperature can be easily calculated, these measurements also allowed us to extract a value for the width of our Gaussian apparatus function, which was quantified as 0.0021 ± 0.0001 cm^{-1} FWHM.

- The determination of the optimum energy level for the pump pulses. While higher energies produce larger Raman signals, the spectral profiles also start to experience broadening and develop an asymmetry due to the AC Stark effect induced by the intense electromagnetic field of the laser pulses. Using a variable attenuator, trials were conducted at several pump pulse energies, and 10 mJ was determined to be the highest pulse energy past which —under our focusing conditions— Stark broadening started to be detectable in the line profiles. Consequently, all the spectra recorded for this work have been obtained with an energy of 10 mJ/pulse in the pump beam.

A CO partial pressure of 5% was used in all the CO-N_2 gas mixtures at all temperatures. The mixtures were prepared *in situ* in the same sample cell used to register the spectra and pressures were monitored at all times by means of capacitive gauges. After performing several tests, the following nominal pressure values were selected at each temperature:

- At 298 K, spectra were recorded at 20, 50, 80, 120 and 160 mbar of total pressure.

- At 195 K, spectra were recorded at 10, 25, 50, 80 and 110 mbar.

- At 77 K, spectra were recorded at 5, 12.5, 20, 30, 40 and 60 mbar.

Every spectrum was recorded at least twice at each nominal pressure. The scan speeds were adjusted according to the width of the spectral lines being registered, typically between 30 and 60 MHz/s. This translated into the experimental line profiles being sampled with between 40 and 60 points per FWHM.

2.2. Experimental results

Figure 2 presents three Q-branch spectra of CO perturbed by N_2 recorded in the course of this work, each one of them registered at one of the three selected temperatures. The nominal pressures of the spectra in the figure have been chosen so that the number densities of CO in the sample cell were similar for the three spectra, and they have been normalized to have the same maximum height. A simple visual inspection of the baseline noise reveals how, as temperature is reduced, the signal-to-noise (S/N) ratio of the spectrum improves due to the total population of the v= 0 vibrational level being distributed among fewer rotational states. An additional contributing factor is that the peaks in the three spectra being compared get slightly narrower due to the diminishing Doppler width.

For the 298 K spectra, rovibrational lines from Q(0) to Q(19) of the band could be registered with a good enough S/N ratio to provide reliable broadening data at all the pressures detailed at the end of Sec. 2.1. This interval is reduced to Q(0)-Q(15) at 195 K and Q(0)-Q(11) at 77 K. Despite the relatively low pressures used, the close proximity between rovibrational components in the band is enough to also produce detectable line interference, especially in the band head. We were able to obtain line mixing coefficients for all lines between Q(0) and Q(8) at 77 K and between Q(0) and Q(5) at 195 K. At 298 K, the poorer S/N ratio of the spectra prevented a similar determination, so we are unable to provide line mixing coefficients at this temperature.

The initial analysis of the line profiles in the spectra was carried out by performing multi-peak fits of the whole Q-branch spectrum. This procedure was conducted independently for each spectrum obtained at a given temperature and pressure. For the selection of the profiles used in the fits, and given that our spectra were obtained in a relatively low presure range and that the two colliding molecules have the same mass, we initially considered a soft-collision (Galatry) profile. However, after testing the profile with different

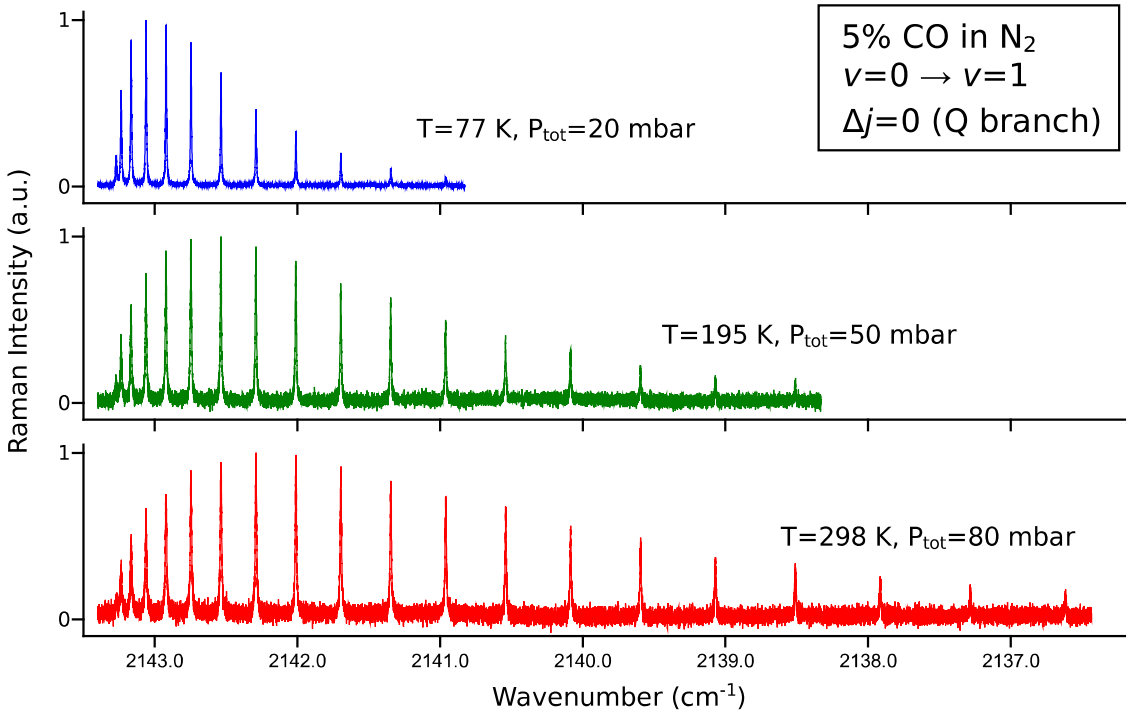

Figure 2: Q-branch spectra of the fundamental band of CO perturbed by N_2 at 77, 195 and 298 K. The nominal pressures have been selected to provide similar number densities.

isolated lines in the spectra at different pressures, it became clear that no significant deviation from a Voigt profile (i.e., no Dicke narrowing) could be detected, at least under our experimental conditions and S/N ratio. Thus, Voigt profiles were selected for the fits. Notice that this initial analysis does not take into account the possible existence of line mixing.

The Voigt fits were initially conducted with both the Gaussian and Lorentzian widths left unconstrained for each line. After verifying that the Gaussian widths obtained across the whole band matched the one previously determined from the spectrum of pure CO at that temperature within the error of the fit for most of the lines, these Gaussian widths were constrained to that value for all lines and the Voigt fits were repeated, this time with only the Lorentzian width unconstrained. This procedure allows a more accurate determination of the Lorentzian widths of the weakest lines in the band, as well as being particularly useful when there is a large difference between the

Gaussian and Lorentzian contributions to the line profile. Figure 3 presents an example of one of the Voigt fits of an isolated rovibrational line at 195 K. No special pattern can be observed in the residuals.

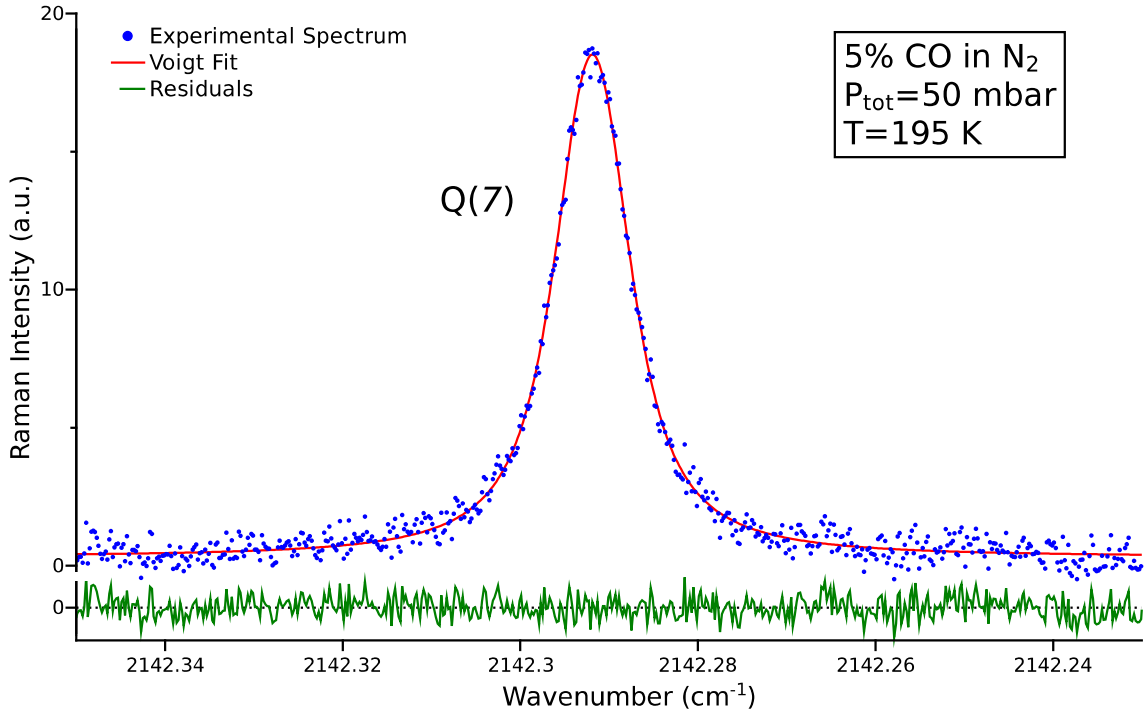

Figure 3: Example of a Voigt fit of the Q(7) rovibrational line at 195 K and a total pressure of 50 mbar. The Gaussian and Lorentzian widhts are 0.00450 and 0.00795 cm^{-1} respectively. Residuals are plotted in the same vertical scale as the experimental spectrum.

Following this fitting procedure, a set of Lorentzian widths at different pressures is extracted for each rovibrational component of the band at each temperature. These widths are then subjected to a simple linear fit, the slope of which renders the collisional broadening coefficient for each line. Figure 4 presents an example of the fits corresponding to the Q(4) line at the three temperatures of reference. It is clearly visible how the error bars assigned to the experimentally determined half widths at half maximum (HWHM) are larger for the higher temperatures. Despite this, and except for the first lines of the band —for which line mixing is noticeable as discussed below—, the variation of the collisional widths with pressure is remarkably well fitted by this linear model in the range of pressures under study.

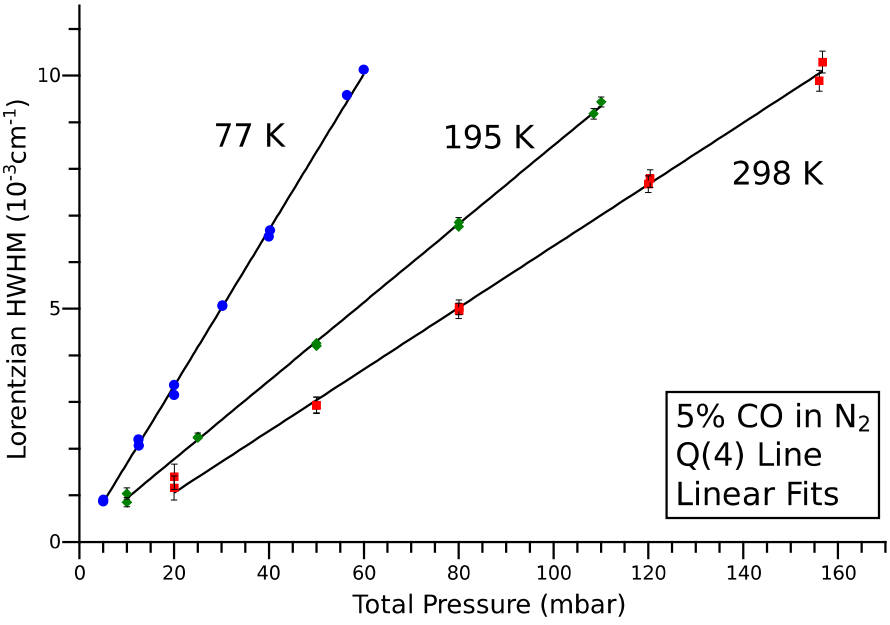

Figure 4: Variation of the Lorentzian HWHM with pressure for the Q(4) line at the three experimental temperatures. The black lines represent linear fits of the data at each temperature. Error bars represent 1 standard error. Due to the small magnitude of the error intervals they are contained within the symbols at 77 K.

For the very first lines of the band, however, the residuals indicate that the use of Voigt profiles is not totally satisfactory. The effect, although subtle in our spectra at the relatively low pressures at which we have worked, indicates the presence of line mixing and is especially visible at 77 K due to the more favorable S/N ratio. Line mixing can be thought of as the consequence of an interference between the different paths that a molecule in a certain initial state can take to reach a final excited state (v= $0, j = j \rightarrow$ v= 1, $j = j$ in our Q-branch example) when it is optically excited in the presence of significant collisional relaxation. Molecular collisions open new potential transition paths in which —for example— a molecule in v= $0, j = j$ could first be collisionaly promoted to v= $0, j = j + 1$, then undergo radiative excitation (in our case via a Raman process) to v= $1, j = j + 1$, and finally relax, again through collisions, to v= 1, $j = j$. This is an alternative path to the direct optical one with the same departure and destination states and with the optical part of the excitation having taken place through a differ-

ent Q-branch transition. The presence of these alternative paths creates an interference that appears as cross-terms in the calculation of the transition probabilities [48, 49]. In density matrix formalism, this phenomenon is characterized as a flow between different components of the optical coherence, i.e., the off-diagonal terms of the density matrix which couple different states of the active molecule, mediated by collisions [50, 51].

From an observational point of view, line mixing manifests itself as a transference of intensity from one region of the spectrum to another, thus altering the overall shape of the spectral band, sometimes dramatically if the coupling between lines is very strong. In a case like ours, in which the low pressures used produce only moderate line overlapping, the coupling is weak and an adequate line mixing model, as confirmed by prior works on this very band [52, 53], is the profile of Rosenkranz [54]. Following Eq. (17) in Ref. 53 and Eq. (1) in Ref. 55 the intensity profile of the band at a given pressure can be described by the expression

$$I(\omega) = \sum_j S_j \frac{\Gamma_j + Y_j\,(\omega - \omega_j - \Delta_j)}{(\omega - \omega_j - \Delta_j)^2 + \Gamma_j^2}. \tag{1}$$

In this expression S_j are the line weights, Γ_j and Δ_j are the collisional linewidths (HWHM) and shifts, ω_j are the central frequencies of the unperturbed lines and Y_j are the line mixing coefficients. The parameters Γ_j, Δ_j and Y_j have a linear dependence with pressure in Rosenkranz's first-order approximation [54]. The shape of the whole band can thus still be calculated as a sum of the independent contributions of each rovibrational component, which can in turn be separated into one Lorentzian and one dispersive contribution. This expression accounts for the purely collisional contribution to the experimental linewidths: in order to compare it to the experimental spectra, the result of Eq. (1) needs to be convolved with the Gaussian contributions (Doppler + apparatus function) present in our spectra. To this end, a minimization Matlab code was developed to calculate a synthetic Rosenkranz profile according to Eq. (1), perform the convolution with the known Gaussian component numerically, and find the values of the parameters in Eq. (1) that minimize the difference between the calculated and experimental bands. When this code is run on an experimental spectrum, we obtain fitted values for the Y_j line mixing coefficients and Γ_j Lorentzian linewidths of each Q(j) rovibrational component of the band at that pressure and temperature. Line shifts in this band are expected to be between one and two orders of mag-

nitude smaller than line broadenings [56–60], so we ignore them by simply considering $(\omega_j - \Delta_j)$ a single parameter in the fit. For a given rotational component Q(j) at a given temperature several Y_j are obtained, one for each pressure at which the band has been recorded. By simply performing a linear fit of these Y_j coefficients against the pressure we obtain as slope a pressure-independent line mixing coefficient for that rotational line that we denote by Y_j^p, with $Y_j^p \cdot p = Y_j$.

The procedure described above was attempted with all the spectra recorded for this work at all temperatures, but the S/N ratio of the 298 K spectra did not allow a reliable determination of the line mixing coefficients from the experimental data. We have been able to obtain values for the coefficients and their associated collisional linewidths for the rovibrational lines between $j = 0$ and $j = 8$ at 77 K and between $j = 0$ and $j = 5$ at 195 K. An example of one of the fits of the experimental spectra, in this case at 77 K, is presented in Fig. 5, with the Lorentzian and dispersive contributions to the overall fit displayed separately. As expected, the Raman scattering is sublorentzian in the high wavenumber side of the band head while it is superlorentzian in the first microwindows.

The deviations of the Lorentzian linewidths Γ_j obtained from convolved Rosenkranz profiles with respect to the ones obtained with Voigt profiles are noticeable only for the first rovibrational lines of the band, with Q(0) being the most affected one. They become negligible, for our standard error intervals, beyond Q(3), where the widths determined by both the Voigt and Rosenkranz models converge. To illustrate the error introduced by the hypothetical neglect of line mixing in the analysis of these first components, Fig. 6 presents, for Q(0) at 77 K, a comparison between the Lorentzian linewidths extracted from the spectra at different pressures with the Voigt and Rosenkranz models. When a linear fit is used on both sets of data to determine the collisional broadening coefficient it is clear that the Voigt data consistently underestimates the width of the rotational line. Since the effect grows markedly with pressure, the widths at higher pressures are more affected and a "blind" linear fit of Voigt data would end up yielding a significantly lower (∼20%) value for the collisional broadening coefficient for this line.

Experimental values for the collisional broadening coefficients of CO perturbed by N_2 at 77, 195 and 298 K are plotted on Fig. 7. The coefficients at 77 and 195 K have been obtained using the Rosenkranz model described above, which renders the same result as a multi-peak Voigt fit for $j > 3$,

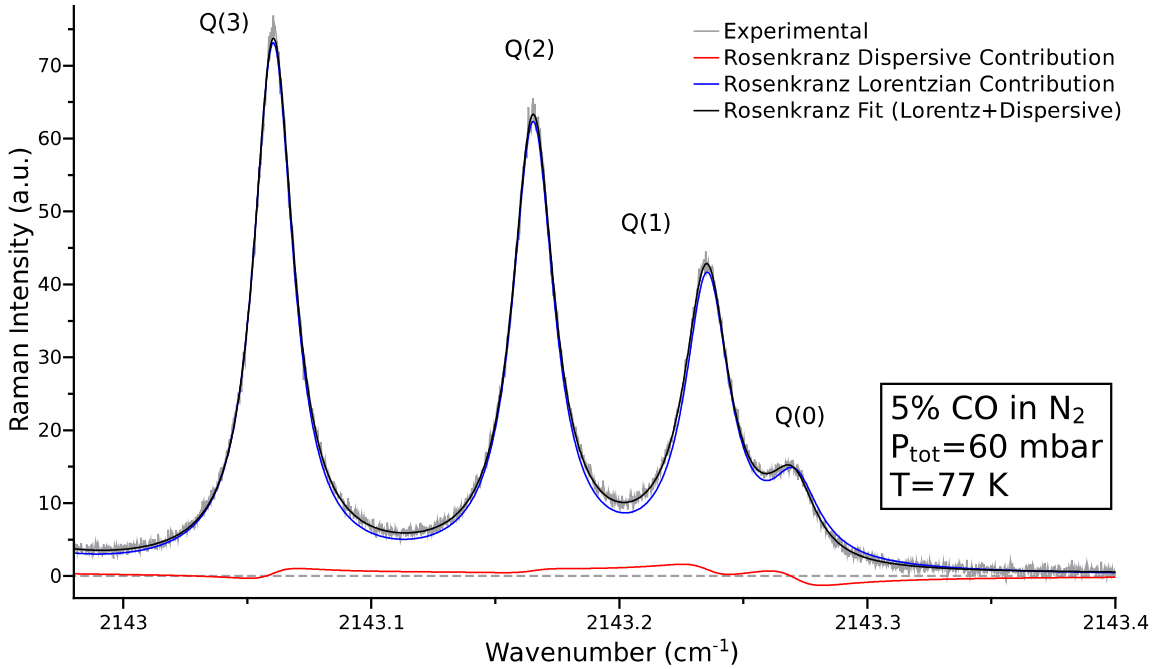

Figure 5: Rosenkranz fit of the first CO Q-branch lines at 77 K and a total pressure of 60 mbar. The Lorentzian and dispersive contributions to the overall Rosenkranz profile are displayed separately to illustrate their relative magnitudes. They have already been convolved with a Gaussian function of 0.0033 cm^{-1} FWHM in order to reproduce the experimental data.

while the ones at 298 K have been obtained with Voigt profiles.

Figure 8 presents the values obtained for the Y_j^p line mixing coefficients. It is clear that the effect of line mixing in the spectrum is more noticeable in the first lines but becomes smaller as j grows and line overlap decreases.

The determination of the theoretical values reported in Figs. 7 and 8 is discussed in the next section. Before doing so, some experimental aspects merit to be further discussed. We considered but rejected the possibility of introducing a correction in the coefficients to account for CO self-perturbation: according to the bibliographic data available at 298 K, both experimental [52] and calculated [38], the line broadening coefficients for the Raman lines of pure CO in its Q branch have values that are only between 1 and 10% higher, depending on the rotational quantum number, than the coefficients we have obtained for the same lines in the CO-N_2 system. That the difference is small is not surprising given that both molecules have similar masses

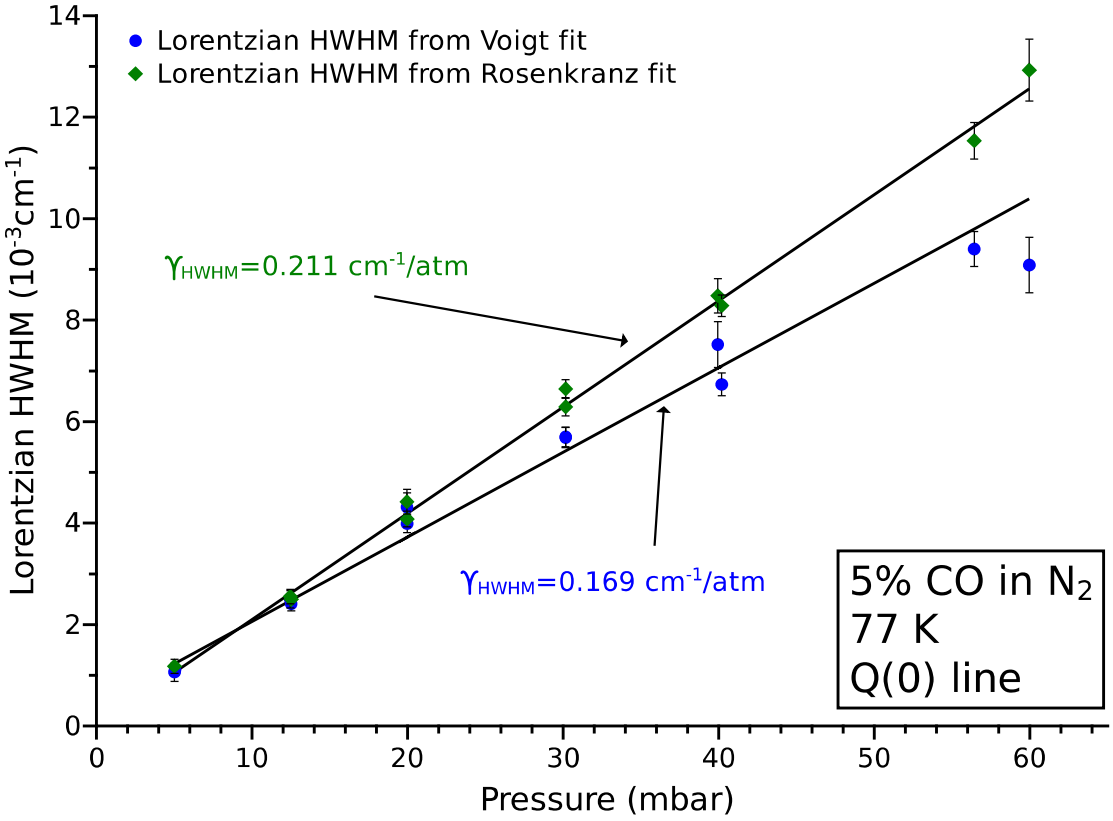

Figure 6: Comparison of linear fits of the collisional HWHMs extracted for Q(0) at 77 K using a Voigt profile (circles) and a Rosenkranz profile (diamonds). Error bars represent 1 standard error.

and the dipole moment of CO is rather weak. Since our CO-N_2 mixtures contain a 5% of CO, and working under the assumption of a simple additive behavior, our experimentally determined coefficients for CO-N_2 would be overestimating the "real" coefficients by a maximum of 0.5% in the worst case. This is significantly smaller than the uncertainty associated to our measurements (see Fig. 7). One final aspect that needs to be addressed in order to perform a comparison between our experimental broadening and mixing coefficients and calculated ones is the influence of the experimental polarization arrangement on the isotropic/anisotropic origin of the intensity of the spectral lines. Besides the population and degeneracy of the rovibra-

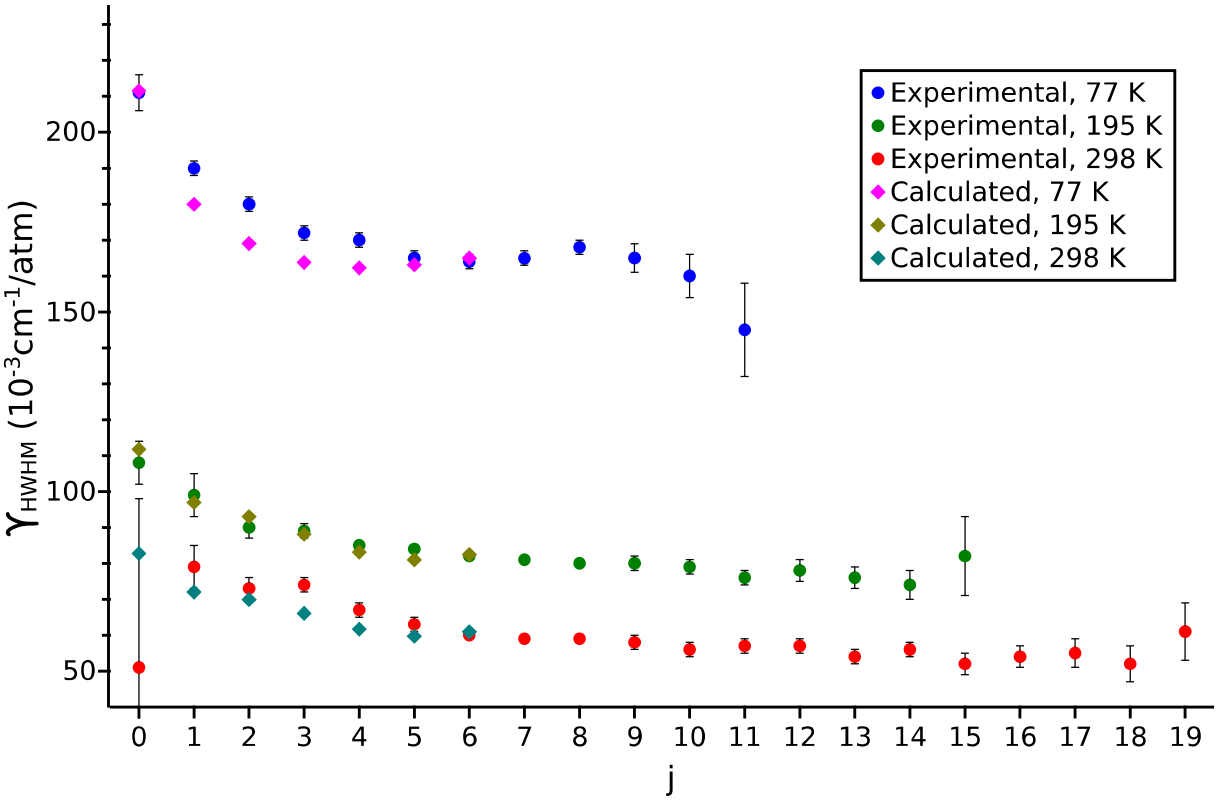

Figure 7: Comparison between experimental and calculated values for the pressure broadening coefficients of CO in N_2 at 77, 195 and 298 K. Error bars in the experimental data represent 1 standard error.

tional levels, the observed intensity of a Q-branch Raman transition depends on the Placzek-Teller coefficients, the polarizability tensor invariants and the polarizations of the excitation and scattered radiations in the experimental layout. For an arrangement with parallel polarizations in the two beams, like the one we have used in this experiment, the dependence of the intensity I_j of a given line Q(j) on these factors is described by the equation [61]

$$I_j \propto \alpha'^2 + \frac{4}{45}\frac{j(j+1)}{(2j-1)(2j+3)}\gamma'^2, \qquad (2)$$

where α' and γ' are the derivatives of the trace and anisotropy invariants, respectively, of the Raman polarizability tensor. From Eq. (2) it clearly

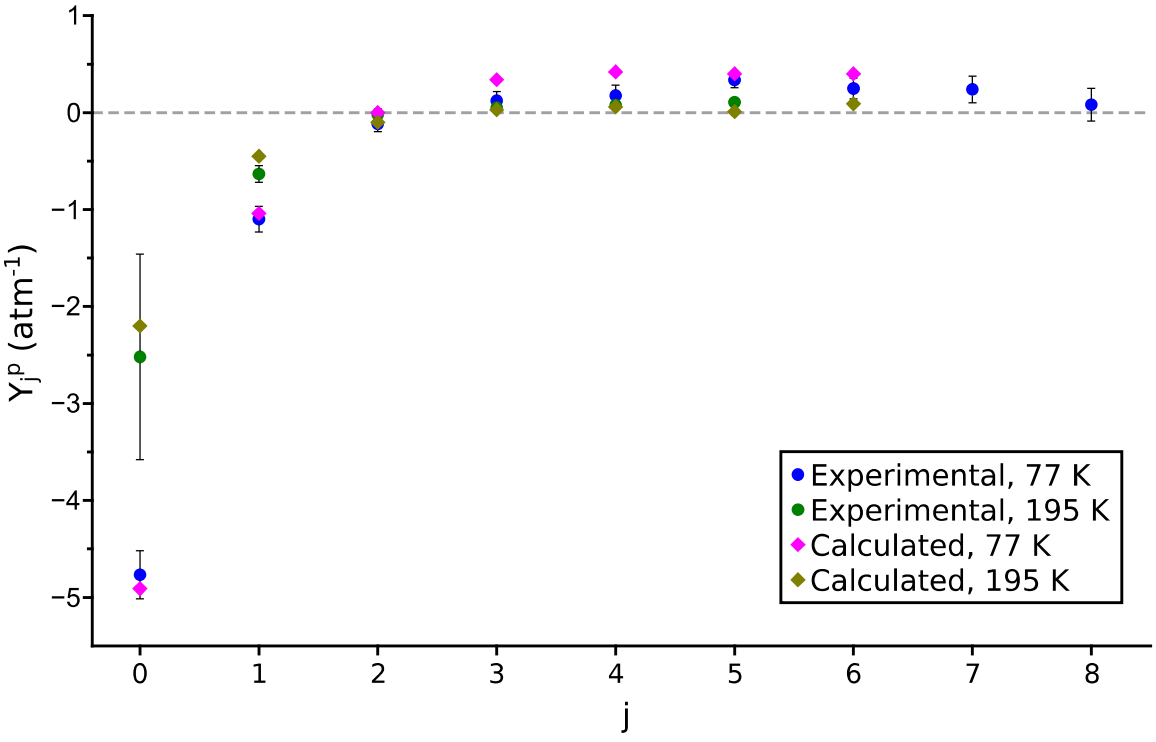

Figure 8: Comparison between experimental and calculated values for the Rosenkranz line mixing coefficients Y_j^p of CO in N_2 at 77 and 195 K. Error bars in the experimental data represent 1 standard error.

follows that the intensity of a Raman Q-branch transition recorded with parallel polarizations has both an isotropic (dependent on α') and an anisotropic (dependent on γ') contribution, with only the Q(0) line being always purely isotropic. In order to calculate these contributions, we rewrite Eq. (2) as

$$I_j \propto 1 + \frac{4}{45}\frac{j(j+1)}{(2j-1)(2j+3)}\left(\frac{\gamma'}{\alpha'}\right)^2. \tag{3}$$

The ratio $\left(\frac{\gamma'}{\alpha'}\right)$ can be obtained from the total band depolarization ratio, defined as

$$\rho = \frac{3\gamma'^2}{45\alpha'^2 + 4\gamma'^2} \tag{4}$$

j	0	1	2	3	4	5	6
I_{ISO}	100%	92.68%	94.66%	95.00%	95.12%	95.18%	95.22%
I_{ANISO}	0%	7.32%	5.34%	5.00%	4.88%	4.82%	4.78%

Table 1: Calculated percentage of isotropic and anisotropic intensity in the Raman Q-branch lines of the CO fundamental recorded with parallel polarizations.

and for which several experimental measurements are available. These have been gathered in a previous work [53], where a value of 2.22 ± 0.05 was proposed for $\left(\frac{\gamma'}{\alpha'}\right)^2$. Based on this number, Tab. 1 presents the calculated percentage of isotropic and anisotropic contributions to the intensity of the first components of the Q branch of CO. It can be seen that the anisotropic contribution is usually very small, of the order of five percent of the total intensity (it approaches 4.7% asymptotically). This is the reason why Q-branch Raman spectra of vibrations with low depolarization ratios like the present one are often approximated as "isotropic spectra", even though technically they are not purely isotropic beyond Q(0). The broadening and mixing coefficients we have obtained experimentally are thus a mixture of isotropic and anisotropic coefficients, but if to the small relative size of the anisotropic contribution we add the fact that the isotropic and anisotropic coefficients are normally very close in value (see for example Ref. 47, where both sets of broadening coefficients are calculated for a different collisional system) we can conclude that for this band our sets of experimental coefficients can be safely compared to isotropic calculated coefficients without introducing significant errors.

3. Theoretical part

3.1. Potential Energy Surface

In the present work, quantum dynamical calculations were performed on the CO-N_2 potential energy surface of Liu *et al.* [2] already described and used by some of us in Ref. [34]. The Jacobi coordinates are described in the two preceding publications. Let us denote the CO and N_2 monomers by the subscripts A and B. The nitrogen molecule bond length is fixed to its experimental ground state value, $r_B = 1.100068$ Å resulting in a 5-dimensional potential $V(r_A, R, \theta_A, \theta_B, \phi)$. This dimension reduction is not a problem in our case, since N_2 is the perturbing molecule and remains in its vibrational ground state in a wide range of temperatures relevant for our spectroscopic

study. The code provided by Liu *et al.* [2] to generate their PES allows to average the PES over the intramolecular CO distance, r_A. We are thus able to consider the CO molecule either in its ground or first excited vibrational states. We furthermore denote this average over the CO vibrational wave functions $\chi_v(r_A)$ with $v = 0$ or 1 by:

$$< V(r_A, R, \theta_A, \theta_B, \phi) >_v = \int_0^\infty \chi_v(r_A) V(r_A, R, \theta_A, \theta_B, \phi) \chi_v(r_A) dr_A. \quad (5)$$

We therefore neglect the rotational dependence of the CO wave functions, a limitation not severe for this molecule in its first rotational states.

For computing facilities these two PESs have been developed over bi-spherical harmonics:

$$< V(r_A, R, \theta_A, \theta_B, \phi) >_v = \sum_{L_A, L_B, L} < V_{L_A, L_B, L}(r_A, R) >_v \; I_{L_A, L_B, L}(\theta_A, \theta_B, \phi). \quad (6)$$

The angular functions are expressed in terms of spherical harmonics tied to the CO and N_2 monomers [34, 45, 62–64]:

$$I_{L_\mathrm{A}, L_\mathrm{B}, L}(\theta_\mathrm{A}, \theta_\mathrm{B}, \phi = \phi_\mathrm{A} - \phi_\mathrm{B}) = \sqrt{\frac{2L+1}{4\pi}} \times \sum_m (L_\mathrm{A}\, m\, L_\mathrm{B}\; -m | L_\mathrm{A}\, L_\mathrm{B}\, L\, 0) Y_{L_\mathrm{A}, m}(\theta_\mathrm{A}, \phi_\mathrm{A}) Y_{L_\mathrm{B}, -m}(\theta_\mathrm{B}, \phi_B), \quad (7)$$

where (....|....) are Clebsch-Gordan coefficients and $|m| \leq \min(\mathrm{L_A}, \mathrm{L_B})$. For computing reasons[1] we have retained 94 potential radial coupling terms for both vibrational states, $< V_{L_A, L_B, L}(r_A, R) >_v$, with L_A = 0,1,...10, L_B = 0,2,...8, $|L_A - L_B| \leq L \leq L_A + L_B$ and $L_A + L_B + L$ even. Following Green [65, 66] and MOLSCAT [67] idiosyncratic normalisation, the radial terms were obtained via Gauss-Legendre quadratures over the θ's and a Chebyshev quadrature over ϕ:

[1] Close coupling calculations are very time consuming and moreover we encountered memory size problems using more terms in this expansion

$$< V_{L_{\rm A},L_{\rm B},L}(r_A,R) >_v = \frac{8\pi^2}{2L+1}$$
$$\times \int_0^{2\pi} {\rm d}\phi \int_{-1}^{+1} {\rm d}(\cos\theta_{\rm A}) \int_{-1}^{+1} {\rm d}(\cos\theta_{\rm B}) < V(r_A,R,\theta_{\rm A},\theta_{\rm B},\phi) >_v I_{L_{\rm A},L_{\rm B},L}(\theta_{\rm A},\theta_{\rm B},\phi). \quad (8)$$

The first radial coupling terms are presented in Fig. 2 of Ref. [34] They were generated on a regular grid from 4 to 200 bohrs with a constant step size of 0.2 bohrs.

3.2. Quantum dynamical methods

In order to obtain scattering matrix elements to derive the line shape parameters (see below) we have used (for historical reasons) both the MOLSCAT code 14 [67] and the version recently published by Hutson and Le Sueur [68]. The close coupling (CC) method is the most accurate but unfortunately also the most time consuming. For the present system, as already discussed by Jóźwiak et al. [34] such calculations are not easy to carry[2] despite the ortho/para disparity in nitrogen that allows us to perform separate calculations for CO-oN_2 and CO-pN_2. Neglecting any vibrational coupling terms we have performed four sets of calculations: two for CO-oN_2 or -pN_2 with the CO molecule in either v= 0 or v= 1. Close coupling calculations were performed for total energies from 0.1 cm^{-1} to a maximum of 300 cm^{-1} and the coupled states approximation (CSA) was used up to 506 cm^{-1}. Above this energy even the CSA is too time consuming. Readers interested in the CSA may consult Ref. [34] and references therein. The necessary generalized cross sections to compute the line shape parameters were obtained by different methods described in the next sections.

3.3. Generalized Cross sections

Following the pioneering work of Hess [69], the so-called generalized Hess method (GHM) provides the spectroscopic cross sections [70, 71] for a spectroscopically active diatomic molecule in a bath of diatomic molecules:

[2] As an example, for CO-oN_2 at a total energy of 300 cm^{-1} with a basis of 417 triplets (j_1, j_2, j_{12}) and a total angular momentum $J = 100$, the number of open channels (j_1, j_2, j_{12}, l) is 3050.

$$\sigma_{\lambda}^{(q)}(v_i j_i^{'}, v_f j_f^{'}; v_i j_i, v_f j_f; j_2, j_2^{'}; E_{kin}) = \frac{\pi}{k^2}(-1)^{(\lambda+j_f-j_f^{'}+j_2-j_2^{'})}\left(\frac{[j_i^{'}]}{[j_i]}\right)^{1/2}$$
$$\times \sum_{\ell,\ell^{'},\bar{\ell},\bar{\ell}^{'}} \left([\ell]\,[\ell^{'}]\,[\bar{\ell}]\,[\bar{\ell}^{'}]\right)^{1/2} i^{(\ell-\ell^{'}-\bar{\ell}+\bar{\ell}^{'})}(-1)^{\ell^{'}-\bar{\ell}^{'}} \begin{pmatrix} \ell & \bar{\ell} & \lambda \\ 0 & 0 & 0 \end{pmatrix} \begin{pmatrix} \ell^{'} & \bar{\ell}^{'} & \lambda \\ 0 & 0 & 0 \end{pmatrix}$$
$$\times \sum_{J,\bar{J}} [J][\bar{J}] \sum_{L,L^{'},\bar{L},\bar{L}^{'}} ([L][L^{'}][\bar{L}][\bar{L}^{'}])^{1/2} \begin{Bmatrix} \lambda & \bar{\ell}^{'} & \ell^{'} \\ j_2^{'} & L^{'} & \bar{L}^{'} \end{Bmatrix} \begin{Bmatrix} \lambda & \bar{\ell} & \ell \\ j_2 & L & \bar{L} \end{Bmatrix} \begin{bmatrix} L & L^{'} & j_f & j_f^{'} \\ \bar{L} & j_i & \bar{L}^{'} & j_i^{'} \\ \lambda & \bar{J} & J & q \end{bmatrix}$$
$$\times \Big[\delta_{j_i j_i^{'}}\delta_{j_f j_f^{'}}\delta_{j_2 j_2^{'}}\delta_{\ell\ell^{'}}\delta_{\bar{\ell}\bar{\ell}^{'}}\delta_{LL^{'}}\delta_{\bar{L}\bar{L}^{'}}$$
$$-\langle v_i j_i (j_2 \ell) L \left| S^{J}(E_{T_{i2}}) \right| v_i j_i^{'} (j_2^{'} \ell^{'}) L^{'} \rangle \langle v_f j_f (j_2 \bar{\ell}) \bar{L} \left| S^{\bar{J}}(E_{T_{f2}}) \right| v_f j_f^{'} (j_2^{'} \bar{\ell}^{'}) \bar{L}^{'} \rangle^{*} \Big]. \tag{9}$$

S-matrix elements are evaluated at the the total energies $E_{T_{i2}} = E_{kin} + E_{v_i j_i} + E_{j_2}$ and $E_{T_{f2}} = E_{kin} + E_{v_f j_f} + E_{j_2}$. k is the modulus of the wave vector associated with the relative collisional energy, $E_{kin} = (\hbar k)^2/2\mu$, with μ the reduced mass of the CO-N_2 system. These cross sections are expressed in Å^2 [72–74]. The vibrational quantum number v_2 has been omitted since it is always 0 in our case for the nitrogen molecule. In Eq. (9), primes indicate post-collisional values, $v_i j_i, v_f j_f$ designates a CO optical transition (denoted $|l\rangle\rangle$ later on) and $v_i j_i', v_f j_f'$ a line ($|l'\rangle\rangle$ later on) to which the line $|l\rangle\rangle$ is coupled by collisions. q designates the line type ($q = 0$ for an isotropic Raman transition, $q = 1$ for an electric dipole transition, $q = 2$ for an anisotropic Raman transition). The coupling scheme is $\vec{j_2} + \vec{\ell} = \vec{L}$, which in turn is coupled to the rotational angular momentum of the active molecule, $\vec{j_i}$, to give the total angular momentum $\vec{J}$. [X] stands for 2X+1, $(: : :)$ refers to the 3-j symbol and $\begin{bmatrix} \vdots & \vdots & \vdots \end{bmatrix}$ to the 12-j symbol of the second kind [75]. Equation (9) leads to two kinds of cross-sections depending on the λ value, the rank of the velocity of the active molecule. For $\lambda = 0$ one recovers [70–72, 76, 77] the standard generalized spectroscopic cross section [48, 49] leading to the relaxation matrix [78, 79]. The simplified expression of Eq. (9) for the diagonal cross sections (pressure broadening and shift) is given by equations 4-6 of Ref. [80] in the case of isotropic Raman Q lines. The $\lambda = 1$ value is associated with velocity-changing collisions. Finally, Eq. (9) is valid

whatever the kind of the optical transition and allows the calculations of both the diagonal and off-diagonal cross sections. Since in the present study we are dealing with the Q lines in Eq. (9) we have $j_i = j_f$ and $j_{i'} = j_{f'}$ as well.

Starting from Eq. (9), specialized to the Q(0) line for which $j_i = j_f = 0$, $v_i = 0$ and $v_f = 1$, we have performed a full CC calculations using our GHM code [81] to determine the diagonal cross sections in the cases λ=0 and λ=1 (note that in MOLSCAT codes the calculation of such cross sections is not implemented). Because the present experiment cannot allow to see the effects of the velocity-changing collisions, tied to λ=1, on the spectral line shapes, the theoretical velocity changing collision frequencies are only presented in Appendix A. The exact pressure broadening coefficients obtained by this method are also provided in this Appendix.

As stated above, for $\lambda = 0$ the real part of the diagonal ($|l\rangle\rangle = |l'\rangle\rangle$) cross section is the pressure broadening cross sections which includes two contributions, one coming from elastic collisions and one coming from the inelastic ones for the active molecule [79, 80, 82–84]. The neglect of the first contribution leads to the so-called random phase approximation (RPA):

$$\sigma_0^{(q)}(v_i j_i, v_f j_f; v_i j_i, v_f j_f; j_2 j_2^{'}) = \\ = \frac{1}{2}\left\{ \sum_{j_1 \neq j_i} \sigma(v_i j_i j_2 \rightarrow v_i j_1 j_2') + \sum_{j_1 \neq j_f} \sigma(v_f j_f j_2 \rightarrow v_f j_1 j_2') \right\}. \quad (10)$$

We furthermore define a partial pressure broadening cross section as

$$\sigma_0^{(q)}(j_i, j_f; j_i, j_f; j_2) = \sum_{j_2'} \sigma_0^{(q)}(j_i, j_f; j_i, j_f; j_2, j_2') \quad (11)$$

whatever the method used for determining it (we have dropped the v's for short). Figures 9 and 10 provide examples of such partial cross sections for the Q(0) and Q(6) lines of the fundamental CO band. One can check that the RPA is accurate for kinetic energies larger than about 50 cm^{-1}, and that the summations of bi-states to bi-states ordinary cross sections are very similar in both vibrational states (v = 0 and 1). The first fact is related to the predominant importance of the inelastic collisions for this system, at least for kinetic energies larger than $\sim$ 50 cm^{-1}, as it is for comparable ones (e.g. CO-Ar [47], CO_2-He [85] or -Ar [86]). The second observation is due to the

fact that the vibrationally averaged PESs in v = 0 and in v = 1 are very similar and that the rovibrational energy levels spacing is very close in both CO vibrational states. Moreover, these figures show that the CSA is quite good, as expected as the kinetic energy and j_2 increase. In addition, even if it is not obvious from these figures, these partial cross sections are very similar as j_2 increases; this point has been extensively discussed for this system in Ref. [34] (see Fig. 6 therein) and shown in previous works (N_2-H_2 [62], C_2H_2 -H_2,-D_2 [45, 87], C_2H_2-N_2 [64] and N_2-N_2 [43]). Consequently, for $j_2 > 7$ we have set the partial pressure broadening cross section (Eq. (11)) equal to a weighted sum of ortho and para contributions determined for $j_2 \leq 7$.

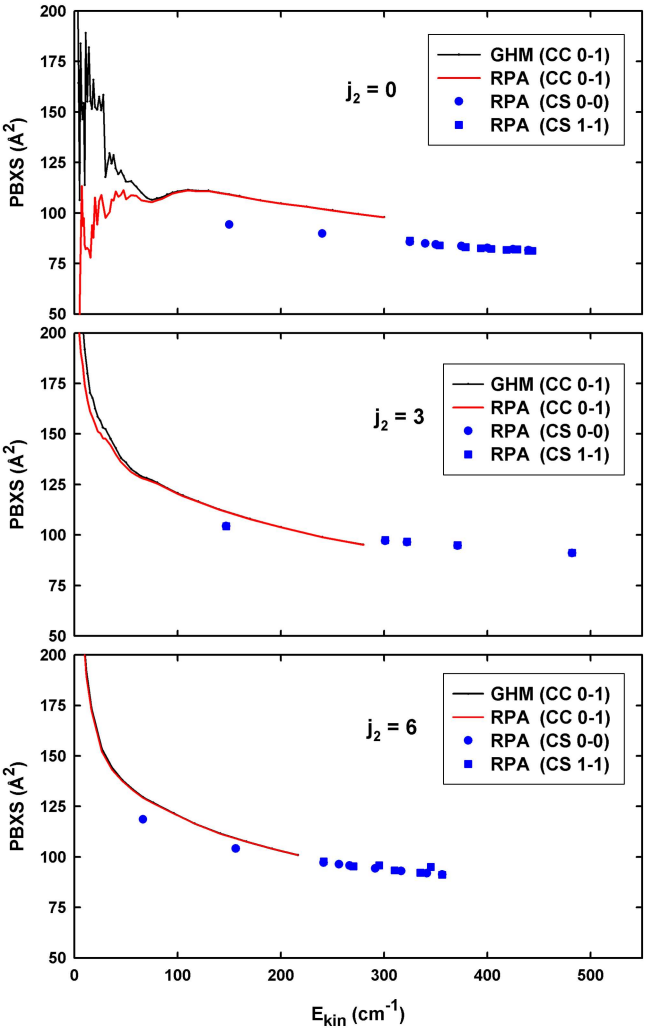

Figure 9: Partial pressure broadening cross sections, as a function of the kinetic energy, for the Q(0) line and $j_2 = 0$, 3 and 6. The black line is the result of our GHM code [81], this is the most exact calculation; red lines are the CC results of the RPA (see text); blue squares and disks are the results of our CSA calculations either in v=0 or in v=1 [88]

.

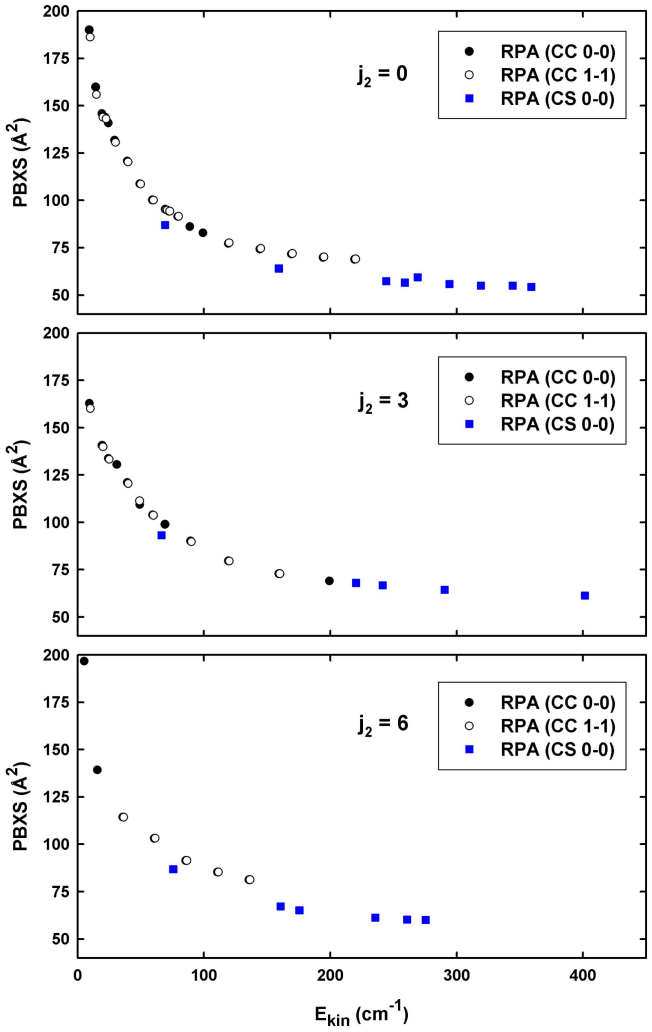

Figure 10: Partial pressure broadening cross sections, as a function of the kinetic energy, for the Q(6) line and $j_2 = 0$, 3 and 6. The black disks result from bi-states to bi-states CC XS in v=0; black circles result from bi-states to bi-states CC XS in v=1; blue squares are the results of our CSA calculations in v=0.

3.4. Relaxation matrix elements

In order to compare the results of our calculations with experimental values we formally construct, within the impact approximation, the relaxation matrix $W_{l'l}$ elements [48, 49, 78, 79]:

$$<< l' \left| W^{(q)} \right| l >> = \frac{n\ \bar{v}_r}{2\pi c} \left\langle \sigma_0^{(q)}(l', l; E_{kin}) \right\rangle \tag{12}$$

where n is the (N_2) density number (assuming that self perturbation is negligible), $\bar{v}_r$ the mean relative speed at the temperature T, and the denominator converts angular frequency to wavenumber (in cm^{-1} with the speed of light c expressed in cm/s). The thermally averaged cross sections over the Maxwell-Boltzmann distribution kinetic energies being given by

$$\left\langle \sigma_0^{(q)}(l', l; E_{kin}) \right\rangle = \sum_{j_2} \rho(j_2) \langle \sigma_0^{(q)}(j_i', j_f'; j_i, j_f; j_2; E_{kin}) \rangle, \tag{13}$$

with the thermally averaged partial cross section

$$\begin{aligned} &\langle \sigma_0^{(q)}(j_i', j_f'; j_i, j_f; j_2; E_{kin}) \rangle = \\ &\quad = \frac{1}{(k_B T)^2} \int_0^\infty E_{kin}\ e^{-E_{kin}/k_B T}\ \sigma_0^{(q)}(j_i', j_f'; j_i, j_f; j_2; E_{kin}) dE_{kin} \end{aligned} \tag{14}$$

and the thermal equilibrium populations given by

$$\rho(j_2) = w_{j_2}(2j_2 + 1) exp(-E_{j_2}/k_B T)/Z(T). \tag{15}$$

The nuclear spin weights w_{j_2} are equal to 2/3 for oN_2 and 1/3 for pN_2; $Z(T)$ is the rotational partition function. Making use of our GHM code [81] we have all the necessary equations to generate the pressure broadening coefficients $\gamma_l = W_{ll}^{(0)}$ for the Q(0) line of the fundamental band of CO at various temperatures. For the other lines (as well also for the Q(0) line for comparison) we made use of the CC and CSA bi-state to bi-state ordinary cross sections. Therefore a few more equations are needed.

For (hypothetical) isotropic Raman lines in a fixed vibrational states a generalized spectroscopic cross section is exactly a negated state to state cross section [48, 66]:

$$\sigma_0^{(0)}(j_1' j_1'; j_1 j_1; j_2 j_2'; E_{kin}) = -\sigma(j_1 j_2 \rightarrow j_1' j_2'; E_{kin}). \tag{16}$$

Moreover, the sum rule is exact [48, 49, 66] leading to the expression of the diagonal relaxation matrix elements in terms of the off-diagonal ones:

$$W_{ll}^{(0)} = -\sum_{l' \neq l} W_{l'l}^{(0)}. \tag{17}$$

The off-diagonal terms being simply a weighted sum of standard rate constants:

$$W_{l'l}^{(0)} = -\sum_{j_2 j_2'} \rho(j_2) R(j_1 j_2 \rightarrow j_1' j_2'). \tag{18}$$

We are now in position to apply the RPA using our CC and CSA rates:

$$\gamma_l = << l \left| W^{(q)} \right| l >> = << v_i j_i v_f j_f \left| W^{(q)} \right| v_i j_i v_f j_f >> =$$

$$= \frac{1}{2} \left\{ << v_i j_i v_f j_i \left| W^{(0)} \right| v_i j_i v_f j_i >> + << v_i j_f v_f j_f \left| W^{(0)} \right| v_i j_f v_f j_f >> \right\}. \tag{19}$$

Note that we have considered that Eq. (19) holds whatever the order of the radiation-mater interaction, q, which is the essence of the RPA. Because the state to state cross sections in v = 0 and in v = 1 are very close we have also performed an average (that is not the RPA) for the off-diagonal relaxation matrix elements:

$$<< l' \left| W^{(0)} \right| l >> = \frac{1}{2} \left\{ << v_i j_i' v_i j_f' \left| W^{(0)} \right| v_i j_i v_i j_f >> \right.$$
$$\left. + << v_f j_i' v_f j_f' \left| W^{(0)} \right| v_f j_i v_f j_f >> \right\}. \tag{20}$$

This allows us to define an averaged line mixing parameter [48, 49, 53, 54, 89, 90] for isotropic Raman Q lines of the fundamental band:

$$Y_{l;0-1\text{band}} = \frac{1}{2} \left\{ Y_{l;v=0} + Y_{l;v=1} \right\} \tag{21}$$

with

$$Y_{l;v} = 2 \sum_{l' \neq l} \frac{W_{l'l;v}}{\sigma_l - \sigma_l'} \tag{22}$$

where σ_i is the line position. Because a relaxation matrix element $W_{l'l;v}$ is derived from rate constants in a given vibrational level, any imaginary part is neglected.

3.5. Theoretical coefficients

Due to our limited grid in kinetic energies, up to 300 cm^{-1} and 506 cm^{-1} for our CC and CSA calculations respectively, in order to perform the thermal average (Eq. 14), the cross sections were extrapolated up to 2000 cm^{-1} using a polynomial form in $a+b/E_{kin}$, where a and b are fitted constants. Therefore our mixed CC/CSA calculations are mainly CC results below 100 K and more affected by the CSA calculations and this extrapolation at 300 K.

First we come back to the Q(0) line of the fundamental band and discuss its pressure broadening coefficients at various temperatures. Figure 11 compares 3 kinds of calculations. As compared to our "exact" GHM calculations this figures shows that the RPA values obtained from our CC set are very good even at the lowest temperature (50 K). Our RPA values deduced from our mixed set of CC/CSA cross sections are in very good agreement with the GHM values except at 50 K for which the agreement is nonetheless not bad. A provides the GHM parameters for the Q(0) line and the table therein shows the detailed comparison for the HWHM determined with the RPA and the GHM. Note that the sum rule, Eq. (17), is verified to better than 5% with our exact GHM coefficients. Recall that the RPA is expected to work better as T and j increase [83, 85, 86, 91]. Therefore, we conclude that our RPA deduced from our CC/CSA calculations should be quite accurate between 50 and 300 K for all the studied lines. Figure 12 displays such results for the Q($j = 0 - 6$) lines.

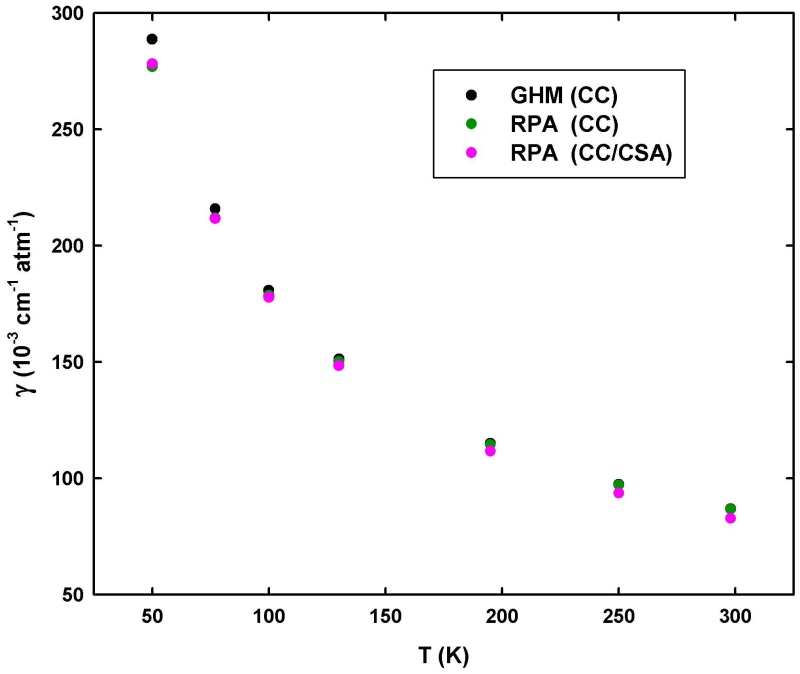

Figure 11: Pressure broadening coefficients at selected temperatures for the Q(0) line of the 0-1 band using the generalized Hess method, the random phase approximation from our CC rates or mixed CC/CSA rates.

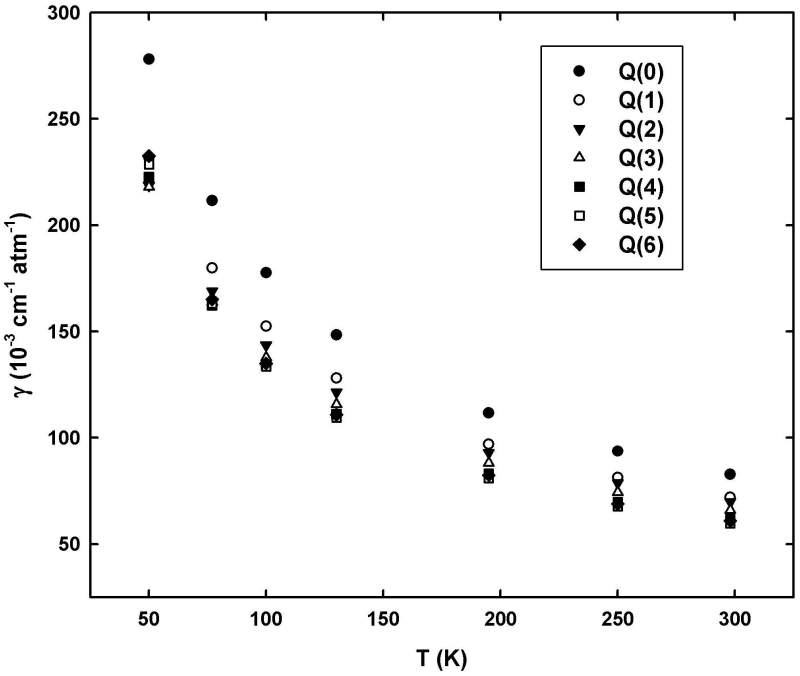

Figure 12: Pressure broadening coefficients at selected temperatures for the Q(0) to Q(6) lines of the fundamental band in N_2 calculated with with our mixed set of CC/CSA rate constants and the RPA.

In order to determine the line mixing coefficients for the Q(0) to Q(6) isotropic Raman lines we have considered a truncated relaxation matrix including the first 11 lines. Convergence tests show that in fact 90% of a line mixing parameter is due to the four neighbouring lines.

As an additional work, on the basis of the RPA, we have calculated the inelastic contribution to the pressure broadening coefficient for pure rotational Stokes lines and electric dipole R lines. Results are given in B.

4. Results and Discussion

The main goal of the work presented in this article is the obtention of collisional line broadening and line mixing coefficients for isotropic Q-branch Raman lines of the fundamental of CO in nitrogen baths at different temperatures. This has been carried out independently from both an experimental and a theoretical point of view as described in the preceding sections. The final results from both approaches are presented jointly in Tabs. 2 and 3. In

order to facilitate their comparison they are also displayed simultaneously in Figs. 7 (broadening coefficients) and 8 (line mixing coefficients).

For the broadening coefficients the results show very good agreement between experiment and calculation. In fact, the agreement is excellent at 195 K, with nearly all the calculated coefficients within the estimated error interval of the experimentally determined values. It is still very good at 77 K, with an average deviation between theory and experiment of only 3.25% (with a maximum of 6.1% for $j = 2$). For 298 K, and if we exclude the coefficient for $j = 0$, whose experimental determination shows a very large uncertainty, the average deviation between experiment and calculation is 6.4% with a maximum of 10.5% for $j = 3$. While not as good as for the other two temperatures, it is still a satisfactory agreement. From Fig. 7 it is also clearly visible that the calculated coefficients are generally very close to the experimental ones for $j = 0$ (again with the exception of 298 K) and $j = 6$ but tend to slighly underestimate them for $j = 1, ..., 4$. This is especially noticeable at 77 and 298 K, since the differences are larger and the pattern easier to see at these temperatures.

The agreement in the line mixing coefficients is also very good, as shown in Fig. 8. The largest relative differences happen at 77 K for $j = 3$ and $j = 4$. The origin of the discrepancy is difficult to pinpoint, as it may lie in either the experimental or theoretical side, or in both of them: from the experimental side, an accurate experimental determination of line mixing coefficients when their values get close to zero, as is the case for these lines, pushes the limits of a technique like SRS, which produces worse S/N ratios than those of typical IR absorption experiments and can be affected by noises of non-statistical nature like drifts in laser power or beam alignment.

From the calculations point of view, the accuracy of the predicted line broadening and mixing coefficients is going to be affected by the approximations used. Namely the use of the random phase approximation, and thus the neglect of the elastic contributions and of a vibrational phase shift, the use of a mixed set of CC/CSA rates and the limitation of our grid in kinetic energies. In particular the neglect of the elastic contributions should lead to an underestimation of the PB (pressure broadening) coefficients at low temperatures. Contrarily, our limited grid will affect more our calculated values as the temperature increases. Despite this, both the calculated pressure broadening and mixing coefficients follow the main trend with both j and T when compared to the present experimental values. Moreover, the line mixing parameters compare well to previous evaluations for the same

	γ_{HWHM} (77 K)		γ_{HWHM} (195 K)		γ_{HWHM} (298K)	
j	Exp.	Calc.	Exp.	Calc.	Exp.	Calc.
0	211(5)	211.5	108(6)	111.7	51(47)	82.7
1	190(2)	180.0	99(6)	96.9	79(6)	72.0
2	180(2)	169.0	90(3)	93.0	73(3)	69.9
3	172(2)	163.8	89(2)	88.1	74(2)	66.1
4	170(2)	162.3	85(1)	83.1	67(2)	61.7
5	165(2)	163.1	84(1)	81.0	63(2)	59.7
6	164(2)	165.0	82(1)	82.4	60(1)	60.9
7	165(2)		81(1)		59(1)	
8	168(2)		80(1)		59(1)	
9	165(4)		80(2)		58(2)	
10	160(6)		79(2)		56(2)	
11	145(13)		76(2)		57(2)	
12			78(3)		57(2)	
13			76(3)		54(2)	
14			74(4)		56(2)	
15			82(11)		52(3)	
16					54(3)	
17					55(4)	
18					52(5)	
19					61(8)	

Table 2: Experimental and calculated collisional broadening coefficients γ_{HWHM} for the Q branch of the v=0→v=1 band of CO in N_2 at 77, 195 and 298 K. Numbers in parentheses are given in units of the last significant digit and represent 1 standard error. Units are $10^{-3}\,\mathrm{cm}^{-1}\,\mathrm{atm}^{-1}$.

	Y_j^p (77 K)		Y_j^p (195 K)		Y_j^p (298 K)
j	Exp.	Calc.	Exp.	Calc.	Calc.
0	-4.8(3)	-4.9	-2.5(11)	-2.2	-1.6
1	-1.1(2)	-1.0	-0.63(9)	-0.5	-0.3
2	-0.12(9)	0.0	-0.02(6)	-0.1	-0.1
3	0.12(9)	0.3	0.05(6)	0.0	0.0
4	0.18(11)	0.4	0.08(6)	0.1	0.0
5	0.34(8)	0.4	0.11(6)	0.0	0.0
6	0.25(11)	0.4		0.1	0.05
7	0.24(2)				
8	0.1(2)				

Table 3: Experimental and calculated Rosenkranz line mixing coefficients Y_j^p for the Q(j) lines at 77, 195 and 298 K (calculated only) in the fundamental band of CO in N_2. Numbers in parentheses are given in units of the last significant digit and represent 1 standard error. Units are atm^{-1}.

band of CO in helium baths [53]. In view of this, the overall present level of agreement found between theory and experiment for the line broadening and mixing coefficients can be considered very satisfactory.

5. Conclusions

The work described throughout this article consists of a joint experimental and theoretical study of the pressure dependence of the shapes of the spectral lines in the rovibrational Raman Q-branch of the CO molecule in a bath of N_2. Quantitative data on line broadening and mixing in the CO-N_2 collisional system at temperatures between 77 and 298 K, in the form of broadening and mixing coefficients, have been obtained in parallel by both the experimental and theoretical branches of the study. These coefficients and the comparison between their experimental and calculated values constitute the main result of this work.

From the experimental point of view, the CO-N_2 collisional system had never before been studied by rovibrational Raman spectroscopy with this level of instrumental resolution. Furthermore, the few experimental studies of the system available in the bibliography do not provide broadening or

mixing coefficients for this band. We are thus presenting a completely new and valuable experimental data set from which future studies using Raman spectroscopy can benefit.

From the theoretical point of view, this is also the first time that advanced, quantum dynamical calculations are used to obtain broadening and mixing data on this Raman band in the CO-N_2 collisional system, since previous studies made use of semiempirical methods. The advanced calculation methodology has been coupled with the use of a very modern, state-of-the-art PES. The very good agreement found between our experimental and theoretical results is a robust indication of the accuracy of the methodologies used and, especially, of the reliability of the data sets obtained. The results presented here might also be considered as yet another validation of the PES of Liu et al. [2].

Regarding the potential impact of our results, the CO-N_2 collisional system is present in a number of different fields, as reviewed in the introduction. Future studies in these fields can benefit from our data. Any measurements using rovibrational Raman spectroscopy (typically CARS) to determine the concentration of CO in a CO-N_2 mixture can use our broadening and mixing coefficients to this end. In the case of combustion studies, which generally take place at higher temperatures than the ones covered in this study, the fact that our data have been obtained at several temperatures can be used for an extrapolation of the coefficients to the region of interest using the well-known temperature power law for the pressure broadening coefficients

The knowledge of broadening and line mixing coefficients is also necessary for an adequate modeling of planetary atmospheres, both terrestrial and of other bodies, in which the presence of CO and N_2 has been detected. Since most atmospheric and astrophysical spectroscopic measurements are carried out by means of absorption techniques (infrared or microwave), the additional theoretical values reported for the pure rotational R- and S- lines might be of particular importance. For instance, the results reported here can be used as initial parameters in a fit of experimental spectra (both pure rotational and, due to a small contribution from the rovibrational phase-shift, of the fundamental band).

Finally, the values we have determined may be also used as a reference data for future theoretical studies of line-shape parameters of rovibrational transitions.

6. Acknowledgement

D. Paredes-Roibás and R. Z. Martínez acknowledge the funding received from Project FIS2017-84391-C2-1-P of Ministerio de Economía y Competitividad. H. Jóźwiak's contribution is supported by the National Science Centre in Poland through Project No. 2018/31/B/ST2/00720.

A. Additional close coupling line shape parameters for the Q(0) line

In this first appendix we provide the line shape parameters, excluding the line mixing one, at various temperatures for the Q(0) line as deduced from our close coupling calculations and the GHM method. We remind the reader that the frequency of the velocity changing collisions leading to the Dicke narrowing are given by [73, 74, 92, 93]:

$$\tilde{\nu}_{opt} \equiv \tilde{\omega}_R - \tilde{\omega}_A. \tag{S1}$$

In Hess notations [69, 71] $\tilde{\omega}_A \equiv \tilde{\omega}_0^{00}(q)$ is nothing else but the complex diagonal relaxation matrix element $(\gamma - i\delta)$ and the relaxation frequency $\tilde{\omega}_R$ is linked to the combined effect of the translational and internal motions. It is expressed in terms of two, mass weighted, collision integrals:

$$\tilde{\omega}_R = n_b \frac{m_a}{m_a + m_b} \tilde{\omega}_0^{00}(q) \; + \; \frac{2}{3} n_b \frac{m_b}{m_a + m_b} \tilde{\omega}_1^{11}(q), \tag{S2}$$

where m_a is the mass of the optically active molecule (CO) and m_b the mass of the perturber (N_2). The collision integrals [94] are derived from the GHM cross sections (Eq. (8)):

$$\tilde{\omega}_\lambda^{s,s'}(q) = \bar{v}_r \int dx x^{(s+s'+2)/2} e^{-x} \sigma_\lambda^{(q)} \left(E_{kin} = x k_B T\right). \tag{S3}$$

Table 4 gathers the line shape parameters as provided by the GHM method for the Q(0) line of the fundamental of CO in N_2. One can see that the RPA slightly underestimates the actual PB coefficients, especially at the lowest temperatures. Moreover, the magnitude of the line shift, due to the difference of the crossed products of elastic scattering amplitudes in the ground and excited vibrational states (equation 6a of Ref. [80]), is smaller than 5% of the PB coefficients, justifying a posteriori their neglect in the experimental work. Finally, the effect of the velocity changing collisions has

been disregarded in the experimental spectra but Table 4 shows that in fact the real part of the complex Dicke parameter is not negligible (for comparison with a similar system, CO in argon baths, see Ref. [95]).

Table 4: Line shape parameters for the Raman Q(0) line of the fundamental band of CO in N_2, in $10^{-3}\,cm^{-1}\,atm^{-1}$, and for selected temperatures: pressure broadening coefficients (γ_0) (and the RPA value), pressure shift coefficients (δ_0), real and imaginary parts of the complex Dicke parameter ($\tilde{\nu}_{opt}$).

T(K)	RPA	γ_0	δ_0	$\widetilde{\nu}^{\rm r}_{\rm opt}$	$\widetilde{\nu}^{\rm i}_{\rm opt}$
50	276.9	288.7	-13.4	46.9	4.8
77	211.8	215.9	-6.9	31.4	1.8
100	178.7	180.8	-4.9	25.0	1.0
130	150.1	151.3	-3.5	20.2	0.5
195	114.5	114.9	-2.3	15.2	0.1
250	97.1	97.4	-1.9	13.2	0.0
298	86.6	86.8	-1.6	12.0	0.0

B. Pressure broadening coefficients for S and R lines

In this second appendix we provide the inelastic contributions to the pressure broadening coefficients, at 77, 195 and 298 K, for the first pure rotational Stokes and R lines. These values are obtained from our mixed CC/CSA set of rate constants used in conjunction with the random phase approximation (Eq. (18)). It is well know that if vibration and rotation-vibration interaction is neglected (i.e. in a rigid rotor approximation) the collisional width of an isotropic Raman line is exactly given by inelastic events. For R and S lines, in addition to the inelastic contribution, the elastic events come into play through reorienting collisions. Such data for R lines are obviously interesting for remote sensing of the atmosphere, while the HWHM of pure rotational S lines may be of interest for the study of combustion processes. Our data, considered as primary pressure broadening coefficients, are not expected to be highly accurate, but may serve as initial parameters in a fit of experimental spectra. One may also use them to guess the temperature dependence of the pressure broadening coefficients essentially between 195 and 300 K. Finally, note that the inelastic contributions are roughly the same (to

about a few percent) for lines of the fundamental band because of the weak vibrational dependence of the PES and a small change of the CO rotational constant in the excited vibrational state. However, for the fundamental band of CO the vibrational dependence of the interaction potential will induce an additional elastic rovibrational dephasing contribution through the S-matrix elements involved in the expression of the generalized spectroscopic cross section (Eq. (9)). Nevertheless, this contribution is expected to be quite small above room temperature, as is the reorientational contribution (the latter being more true as j increases).

Table 5 provides the results for Raman S lines. Unfortunately, we are not aware of experimental measurements to compare with, although we note that Hsu et al. [36] reported the data for the pure rotational S(6-15) lines. Table 6 provides our results for R lines. They are compared with experimental values available in the literature for the pure rotational R(0), [26–29] R(1), [29, 30] R(2) [29, 31] and R(4) [32, 33] lines and with our CSA calculations from the previous work [34]. In the latter case, we refer to the values of γ_0 and $\gamma^\dagger$ (collisional width which includes the effect of speed-dependence of the broadening, see Sec. IV in Ref. [34]), obtained from the PES of Liu et al. [2]. Values of the pressure broadening coefficients at 195 K were determined from Refs. [26–28, 30, 31, 34] using the power-law dependence of $\gamma_0(T)$. We note that the values from Refs. [29] and [33] are reported for the ^{13}CO molecule, although, as pointed out by the authors, the dependence of collisional width on the isotope of carbon is negligible. Lack of isotopic dependence in the pressure broadening coefficients was also observed for the self-broadened OCS lines [29], as well as for the Ar-perturbed lines of CO [96] and He-perturbed lines of CO_2 [97]. Our results also compare quite well with measurements performed in the fundamental band [20–23] and even in the first and second overtones [24, 25].

Table 5: Inelastic contribution to the pressure broadening coefficients, in 10^{-3} cm^{-1} atm^{-1}, for the rotational S(0) to S(4) lines of CO in N_2 at selected temperatures.

T(K)	S(0)	S(1)	S(2)	S(3)	S(4)
77	190.0	171.8	165.6	163.3	163.3
195	102.7	93.1	88.2	84.3	82.0
298	76.8	69.7	65.9	62.7	60.6

Finally, our calculated values for Q and R lines agree quite well with the

most recent extensive calculations [38] performed on the basis of the semi-classical Robert-Bonamy formalism using a semi-empirical PES, the isotropic part of which was adjusted to match experimental data. These authors have shown that, at room temperature, the elastic reorientational contribution to the linewidth of the S (and thus R) lines is smaller than 3×10^{-3}cm^{-1}atm^{-1} for j$<$4 and smaller than 1×10^{-3}cm^{-1}atm^{-1} for higher j's, thus justifying the RPA.

Table 6: Inelastic contribution to the pressure broadening coefficients, in $10^{-3}\,cm^{-1}\,atm^{-1}$, for the rotational R(0) to R(5) lines of CO in N_2 and a comparison with the experimental data at selected temperatures.

T(K)		R(0)	R(1)	R(2)	R(3)	R(4)	R(5)
77	This work	195.6	174.4	166.2	163.0	162.6	163.6
195	This work	105.6	95.5	90.1	85.8	82.3	80.5
	Ref. 26	104.2					
	Ref. 27	119.7					
	Ref. 28	109.06					
	Ref. 30		104.9				
	Ref. 31			101.7			
	Ref. 34	117.98					
	Ref. 34[a]	112.82					
298	This work	78.9	71.8	67.8	64.1	61.1	60.3
	Ref. 26	76.2					
	Ref. 27	83.1					
	Ref. 28	79.70					
	Ref. 29[b]	78.80	73.45	69.65	68.90		
	Ref. 30		76.6				
	Ref. 31			71.14			
	Ref. 32[c]					66.1	
	Ref. 33[b]					64.0	
	Ref. 34	87.31					
	Ref. 34[a]	83.49					

[a]Calculations including the speed-dependence of the broadening.
[b]Measurements performed for ^{13}CO at $T = 296$ K.
[c]Measurements performed at $T = 295$ K.

References

[1] M. H. Karimi-Jafari, A. Maghari, A. Farjamnia, Intermolecular potential energy surface of the N_2-CO dimer: Ab initio investigation and analytical representation, J. Phys. Chem. A 115 (2011) 1143–1151.

[2] J.-M. Liu, Y. Zhai, X.-L. Zhang, H. Li, Intermolecular configurations dominated by quadrupole-quadrupole electrostatic interactions: explicit correlation treatment of the five-dimensional potential energy surface and infrared spectra for the CO-N_2 complex, Phys. Chem. Chem. Phys. 20 (2018) 2036–2047.

[3] L. A. Surin, I. V. Tarabukin, S. Schlemmer, Y. N. Kalugina, A. van der Avoird, *Ab initio* potential and rotational spectra of the CO-N_2 complex, J. Chem. Phys. 148 (2018) 044313.

[4] H. Cybulski, C. Henriksen, R. Dawes, X.-G. Wang, N. Bora, G. Avila, T. Carrington Jr., B. Fernández, *Ab initio* study of the CO-N_2 complex: a new highly accurate intermolecular potential energy surface and rovibrational spectrum, Phys. Chem. Chem. Phys. 20 (2018) 12624–12636.

[5] N. D. Sze, Anthropogenic co emissions: Implications for the atmospheric co-oh-ch_4 cycle, Science 195 (1977) 673–675.

[6] S. C. Wofsy, Interactions of ch_4 and co in the earth's atmosphere, Annu. Rev. Earth Planet. Sci. 4 (1976) 441–469.

[7] T. C. Owen, T. L. Roush, D. P. Cruikshank, J. L. Elliot, L. A. Young, C. De Bergh, B. Schmitt, T. R. Geballe, R. H. Brown, M. J. Bartholomew, Surface ices and the atmospheric composition of pluto, Science 261 (1993) 745–748.

[8] B. L. Lutz, C. De Bergh, T. Owen, Titan: Discovery of carbon monoxide in its atmosphere, Science 220 (1983) 1374–1375.

[9] D. P. Cruikshank, T. L. Roush, T. C. Owen, T. R. Geballe, C. De Bergh, B. Schmitt, R. H. Brown, M. J. Bartholomew, Ices on the surface of triton, Science 261 (1993) 742–745.

[10] N. Madhusudhan, S. Seager, A temperature and abundance retrieval method for exoplanet atmospheres, Astrophys. J. 707 (2009) 24.

[11] R. J. de Kok, M. Brogi, I. A. Snellen, J. Birkby, S. Albrecht, E. J. de Mooij, Detection of carbon monoxide in the high-resolution day-side spectrum of the exoplanet hd 189733b, Astronomy & Astrophysics 554 (2013) A82.

[12] N. Madhusudhan, J. Harrington, K. B. Stevenson, S. Nymeyer, C. J. Campo, P. J. Wheatley, D. Deming, J. Blecic, R. A. Hardy, N. B. Lust, et al., A high c/o ratio and weak thermal inversion in the atmosphere of exoplanet wasp-12b, Nature 469 (2011) 64–67.

[13] C. He, S. M. Hörst, S. Riemer, J. A. Sebree, N. Pauley, V. Vuitton, Carbon monoxide affecting planetary atmospheric chemistry, Astrophys. J. Lett. 841 (2017) L31.

[14] S. M. Hörst, M. A. Tolbert, The effect of carbon monoxide on planetary haze formation, Astrophys. J. 781 (2014) 1–5.

[15] M. Woyde, W. Stricker, The application of cars for temperature measurements in high pressure combustion systems, Appl. Phys. B 50 (1990) 519–525.

[16] R. Hall, Cars spectra of combustion gases, Combust. Flame 35 (1979) 47–60.

[17] D. Klick, K. A. Marko, L. Rimai, Broadband single-pulse cars spectra in a fired internal combustion engine, Appl. Opt. 20 (1981) 1178–1181.

[18] J. H. Stufflebeam, A. C. Eckbreth, Cars diagnostics of solid propellant combustion at elevated pressure, Combust. Sci. Technol. 66 (1989) 163–179.

[19] V. Bergmann, W. Meier, D. Wolff, W. Stricker, Application of spontaneous raman and rayleigh scattering and 2d lif for the characterization of a turbulent $ch_4/h_2/n_2$ jet diffusion flame, Appl. Phys. B 66 (1998) 489–502.

[20] T. Nakazawa, M. Tanaka, Measurements of intensities and self- and foreign-gas-broadened half-widths of spectral lines in the co fundamental band, J. Quant. Spectrosc. Radiat. Transfer 28 (1982) 409–416.

[21] T. Nakazawa, M. Tanaka, Intensities, half-widths and shapes of spectral lines in the fundamental band of CO at low temperatures, J. Quant. Spectrosc. Radiat. Transf. 28 (1982) 471–480.

[22] T. Drascher, T. F. Giesen, T. Y. Wang, N. Schmücker, R. Schieder, G. Winnewisser, P. Joubert, J. Bonamy, Temperature-dependent line shift broadening of co infrared transistions, J. Mol. Spectrosc 192 (1998) 268–276.

[23] A. Predoi-Cross, C. Luo, P. M. Sinclair, J. R. Drummond, A. D. May, Line broadening and temperature exponent of the fundamental band in co-n_2 mixtures, J. Mol. Spectrosc 198 (1999) 291–303.

[24] A. Predoi-Cross, J. P. Bouanich, D. C. Benner, A. D. May, J. R. Drummond, Broadening, shifting, and line asymmetries in the 2←0 band of CO and CO–N_2: Experimental results and theoretical calculations, J. Chem. Phys. 113 (2000) 158–168.

[25] A. Predoi-Cross, C. Hnatovsky, K. Strong, J. R. Drummond, D. C. Benner, Temperature dependence of self- and n_2-broadening and pressure-induced shifts in the $j = 3 \leftarrow 0$ band of co, J. Mol. Struct. 695-696 (2004) 269–286.

[26] B. J. Connor, H. Radford, Pressure broadening of the CO J = 1-0 rotational transition by N_2, O_2, and air, J. Mol. Spectrosc. 119 (1986) 229–231.

[27] J. Colmont, N. Monnanteuil, Self, nitrogen and oxygen broadening of the 115-GHz line of carbon monoxide, J. Quant. Spectrosc. Radiat. Transf. 35 (1986) 81–85.

[28] N. Nissen, J. Doose, A. Guarnieri, H. Mäder, V. N. Markov, G. Y. Golubyatnikov, I. I. Leonov, V. N. Shanin, A. F. Krupnov, Foreign gas broadening studies of the j'←j = 1←0 rotational line of co by frequency and time domain techniques, Z. Naturforsch 54a (1999) 218–224.

[29] C. Puzzarini, L. Dore, G. Cazzoli, A comparison of lineshape models in the analysis of modulated and natural rotational line profiles: Application to the pressure broadening of ocs and co, J. Mol. Spectrosc 216 (2002) 428–436.

[30] N. Semmoud-Monnanteuil, J. Colmont, Pressure broadening of millimeter lines of carbon monoxide, J. Mol. Spectrosc. 126 (1987) 210–219.

[31] D. Priem, F. Rohart, J. M. Colmont, G. Wlodarczak, J. P. Bouanich, Lineshape study of the $j = 3 \leftarrow 2$ rotational transition of co perturbed by n_2 and o_2, J. Mol. Struct. 517-518 (2000) 435–454.

[32] V. N. Markov, G. Y. Golubiantnikov, V. A. Savin, D. A. Sergeev, A. Guarnieri, H. Mädler, Line broadening and shifting studies of the $j = 5 \leftarrow 4$ transition of carbon monoxide perturbed by co, n_2, and o_2, J. Mol. Spectrosc (2002) 1–5.

[33] J.-M. Colmont, L. Nguyen, F. Rohart, G. Wlodarczak, Lineshape analysis of the $j = 3 - 2$ and $j = 5 - 4$ rotational transitions of room temperature CO broadened by N_2, O_2, CO_2 and noble gases, J. Mol. Spectrosc 246 (2007) 86–97.

[34] H. Jóźwiak, F. Thibault, H. Cybulski, P. Wcisło, Ab initio investigation of the CO-N_2 quantum scattering: the collisional perturbation of the pure rotational R(0) line in CO, J. Chem. Phys. 154 (2021) 054314.

[35] M. Afzelius, C. Brackmann, F. Vestin, P.-E. Bengtsson, Pure rotational coherent anti-stokes raman spectroscopy in mixtures of CO and N_2, Appl. Opt. 43 (2004) 6664–6672.

[36] P. S. Hsu, H. U. Stauffer, N. Jiang, J. R. Gord, S. Roy, Direct measurements of collisional raman line broadening in the s-branch transitions of co perturbed by co, n_2, and co_2, Appl. Opt. 58 (2019) C1–C6.

[37] A. Roblin, J. Bonamy, D. Robert, M. Lefebvre, M. Péalat, Rotational relaxation model for co-n_2. prediction of cars profiles and comparison with experiment, Journal de Physique II 2 (1992) 285–294.

[38] M. Afzelius, P.-E. Bengtsson, J. Bonamy, Semiclassical calculations of collision line broadening in Raman spectra of N_2 and CO mixtures, J. Chem. Phys. 120 (2004) 8616–8623.

[39] A. Owyoung, E. D. Jones, Stimulated Raman spectroscopy using low-power cw lasers, Opt. Lett. 1 (1977) 152–154.

[40] R. S. McDowell, C. W. Patterson, A. Owyoung, Quasi-cw inverse Raman spectroscopy of the ν_1 fundamental of $^{13}CH_4$, J. Chem. Phys. 72 (1980) 1071–1076.

[41] P. Esherick, A. Owyoung, High resolution stimulated Raman spectroscopy, volume 9 of *Advances in IR and Raman Spectroscopy*, Heyden, 1983.

[42] R. Z. Martínez, D. Bermejo, P. Wcisło, F. Thibault, Accurate wavenumber measurements for the $S_0(0)$, $S_0(1)$, and $S_0(2)$ pure rotational Raman lines of D_2, J. Raman Spectrosc. 50 (2019) 127–129.

[43] F. Thibault, R. Z. Martínez, D. Bermejo, L. Gómez, Collisional line widths of autoperturbed N_2: Measurements and quantum calculations, J. Quant. Spectrosc. Radiat. Transf 112 (2011) 2542–2551.

[44] R. Z. Martínez, D. Bermejo, Experimental determination of the rate of V–V collisional relaxation in $^{14}N_2$ in its ground ($X^1\Sigma\,^+_g$) electronic state between 77 and 300 K, Phys. Chem. Chem. Phys. 17 (2015) 12661–12672.

[45] F. Thibault, B. Corretja, A. Viel, D. Bermejo, R. Z. Martínez, B. Bussery-Honvault, Linewidths of C_2H_2 perturbed by H_2: experiments and calculations from an ab initio potential, Phys. Chem. Chem. Phys. 10 (2008) 5419–5428.

[46] G. Di Lonardo, L. Fusina, A. Baldan, R. Z. Martínez, D. Bermejo, High resolution infrared and Raman spectroscopy of ν_2 and associated combination and hot bands of $^{13}C^{12}CD_2$, Mol. Phys. 109 (2011) 2533–2542.

[47] F. Thibault, R. Z. Martínez, J. L. Domenech, D. Bermejo, J.-P. Bouanich, Raman and infrared linewidths of CO in Ar, J. Chem. Phys. 117 (2002) 2523–2531.

[48] A. Lévy, N. Lacome, C. Chackerian, Collisional line mixing, in: K. N. Rao, A. Weber (Eds.), Spectroscopy of the Earth's Atmosphere and Interstellar Medium, Academic Press, 1992, pp. 261–337.

[49] J.-M. Hartmann, C. Boulet, D. Robert, Collisional Effects on Molecular Spectra, Elsevier, Amsterdam, 2008.

[50] A. D. May, Molecular dynamics and a simplified master equation for spectral line shapes, Phys. Rev. A 59 (1999) 3495–3505.

[51] A. May, W.-K. Liu, F. McCourt, R. Ciuryło, J. S.-F. Stoker, D. Shapiro, R. Wehr, The impact theory of spectral line shapes: a paradigm shift, Can. J. Phys. 91 (2013) 879–895.

[52] G. J. Rosasco, W. Lempert, W. S. Hurst, A. Fein, Line interference effects in the vibrational Q-branch spectra of N_2 and CO, Chem. Phys. Lett. 97 (1983) 435–440.

[53] J. Boissoles, F. Thibault, J. L. Domenech, D. Bermejo, C. Boulet, J. M. Hartmann, Temperature dependence of line mixing effects in the stimulated raman Q-branch of CO in He: A further test of close coupling calculations, J. Chem. Phys. 115 (2001) 7420–7428.

[54] P. W. Rosenkranz, Shape of the 5 mm Oxygen Band in the Atmosphere, IEEE Transactions on Antennas and Propagation AP-23 (1975) 498–506.

[55] R. Ciuryło, J. Szudy, Line-mixing and collision-time asymmetry of spectral line shapes, Phys. Rev. A 63 (2001) 042714.

[56] N. Anselm, K. Yamada, R. Schieder, G. Winnewisser, Measurements of foreign gas pressure shift and broadening effects in the (1-0) band of CO with N_2 and Ar, J. Mol. Spectrosc. 161 (1993) 284–296.

[57] A. Hamdouni, A. Barbe, J.-J. Plateaux, V. Langlois, V. Dana, J.-Y. Mandin, M. Badaoui, Measurements of N_2-induced shifts and broadening coefficients of lines in CO fundamental from Fourier transform spectra, J. Quant. Spectrosc. Radiat. Transf. 50 (1993) 247–255.

[58] J. Mandin, V. Dana, M. Badaoui, A. Barbe, A. Hamdouni, J. Plateaux, Measurements of pressure-broadening and pressure-shifting coefficients from FT spectra, J. Mol. Spectrosc. 164 (1994) 328–337.

[59] P. Sinclair, P. Duggan, R. Berman, A. May, J. Drummond, Line broadening, shifting, and mixing in the fundamental band of CO perturbed by N_2 at 301 K, J. Mol. Spectrosc. 181 (1997) 41–47.

[60] C. Luo, R. Berman, A. Predoi-Cross, J. Drummond, A. May, Lineshifts in the fundamental band of CO: Confirmation of experimental results for n_2 and comparison with theory, J. Mol. Spectrosc 196 (1999) 290–295.

[61] D. A. Long, The Raman Effect, John Wiley & Sons Ltd., Chichester, West Sussex, England, 2002.

[62] L. Gomez, R. Z. Martínez, D. Bermejo, F. Thibault, P. Joubert, B. Bussery-Honvault, J. Bonamy, Q-branch linewidths of N_2 perturbed by H_2: Experiments and quantum calculations from an ab initio potential, J. Chem. Phys. 126 (2007) 204302.

[63] F. Thibault, L. Gomez, S. V. Ivanov, O. G. Buzykin, C. Boulet, Comparison of quantum, semi-classical and classical methods in the calculation of nitrogen self-broadened linewidths, J. Quant. Spectrosc. Radiat. Transf 113 (2012) 1887–1897.

[64] F. Thibault, R. Z. Martínez, D. Bermejo, S. V. Ivanov, O. G. Buzykin, Q. Ma, An experimental and theoretical study of nitrogen-broadened acetylene lines, J. Quant. Spectrosc. Radiat. Transf 142 (2014) 17–24.

[65] S. Green, Rotational excitation in H_2-H_2 collisions: Close-coupling calculations, J. Chem. Phys. 62 (1975) 2271–2277.

[66] S. Green, Raman linewidths and rotationally inelastic collision rates in nitrogen, J. Chem. Phys. 98 (1993) 257–268.

[67] J. M. Hutson, S. Green, MOLSCAT version 14, Collaborative Computational Project 6 of the UK Science and Engineering Research Council, Daresbury Laboratory, UK (1995).

[68] J. M. Hutson, C. R. L. Sueur, molscat: A program for non-reactive quantum scattering calculations on atomic and molecular collisions, Comput. Phys. Commun. 241 (2019) 9–18.

[69] S. Hess, Kinetic theory of spectral line shapes. The transition between Doppler broadening and collisional broadening, Physica 61 (1972) 80–94.

[70] G. C. Corey, F. R. McCourt, Dicke narrowing and collisional broadening of spectral lines in dilute molecular gases, J. Chem. Phys. 81 (1984) 2318–2329.

[71] L. Monchick, L. W. Hunter, Diatomic-diatomic molecular collision integrals for pressure broadening and Dicke narrowing: A generalization of Hess's theory, J. Chem. Phys. 85 (1986) 713–718.

[72] L. Demeio, S. Green, L. Monchick, Effects of velocity changing collisions on line shapes of HF in Ar, J. Chem. Phys. 102 (1995) 9160–9166.

[73] R. Z. Martínez, D. Bermejo, F. Thibault, P. Wcisło, Testing the ab initio quantum-scattering calculations for the D_2–He benchmark system with stimulated Raman spectroscopy, J. Raman Spectrosc. 49 (2018) 1339–1349.

[74] F. Thibault, R. Z. Martínez, D. Bermejo, P. Wcisło, Line-shape parameters for the first rotational lines of HD in He, Mol. Astrophys. 19 (2020) 100063.

[75] A. P. Yutsis, I. B. Levinson, V. V. Vanagas, Jerusalem: Israel Program for Scientific Translations, 1962.

[76] J. Schaefer, L. Monchick, Line shape cross sections of HD immersed in He and H_2 gas. I. Pressure broadening cross sections, J. Chem. Phys. 87 (1987) 171–181.

[77] J. Schaefer, L. Monchick, Line broadening of HD immersed in He and H_2 gas, Astron. Astrophys. 265 (1992) 859–868.

[78] U. Fano, Pressure broadening as a prototype of relaxation, Phys. Rev. 131 (1963) 259–268.

[79] A. Ben-Reuven, Impact broadening of microwave spectra, Phys. Rev. 145 (1966) 7–22.

[80] R. Blackmore, S. Green, L. Monchick, Polarized D_2 Stokes–Raman Q branch broadened by He: A numerical calculation, The Journal of Chemical Physics 88 (1988) 4113–4119.

[81] F. Thibault, H. Jóźwiak, Code for pressure broadening, shift and complex Dicke cross sections for 2 diatomics, Mendeley Data, V2, doi: 10.17632/tdvgvwr2t7.2, 2021.

[82] M. Baranger, General impact theory of pressure broadening, Phys. Rev. 112 (1958) 855–865.

[83] A. E. DePristo, H. Rabitz, The effect of elastic and reorientation collisions on vibration-rotation lineshapes: A semi-empirical approach, J. Quant. Spectrosc. Radiat. Transf 22 (1979) 65–79.

[84] R. Blackmore, A modified Boltzmann kinetic equation for line shape functions, The Journal of Chemical Physics 87 (1987) 791–800.

[85] F. Thibault, B. Calil, J. Boissoles, J. M. Launay, Experimental and theoretical CO_2–He pressure broadening cross sections, Phys. Chem. Chem. Phys. 2 (2000) 5404–5410.

[86] F. Thibault, B. Calil, J. Buldyreva, M. Chrysos, J.-M. Hartmann, J.-P. Bouanich, Experimental and theoretical CO_2–Ar pressure-broadening cross sections and their temperature dependence, Phys. Chem. Chem. Phys. 3 (2001) 3924–3933.

[87] F. Thibault, E. Fuller, K. Grabow, J. Hardwick, C. Marcus, D. Marston, L. Robertson, E. Senning, M. Stoffel, R. Wiser, Experimental line broadening and line shift coefficients of the acetylene $\nu_1 + \nu_3$ band pressurized by hydrogen and deuterium and comparison with calculations, J. Mol. Spectrosc 256 (2009) 17–27.

[88] F. Thibault, Pressure broadening and shift code for 2 diatomics - coupled states approximation, Mendeley Data, V2,doi: 10.17632/ykxz36nwry.2, 2020.

[89] E. W. Smith, Absorption and dispersion in the O_2 microwave spectrum at atmospheric pressures, J. Chem. Phys. 74 (1981) 6658–6673.

[90] F. Thibault, J. Boissoles, R. Le Doucen, R. Farrenq, M. Morillon-Chapey, C. Boulet, Line-by-line measurements of interference parameters for the 0–1 and 0–2 bands of CO in He, and comparison with coupled-states calculations, J. Chem. Phys. 97 (1992) 4623–4632.

[91] A. E. DePristo, H. Rabitz, On the use of various scaling theories in the deconvolution of rotational relaxation data: Application to pressure-broadened linewidth measurements, J. Chem. Phys. 69 (1978) 902–911.

[92] F. Thibault, K. Patkowski, P. Zuchowski, H. Jóźwiak, P. Wcisło, R. Ciuryło, Rovibrational line-shape parameters for H_2 in He and new

H_2-He potential energy surface, J. Quant. Spectrosc. Radiat. Transfer 202 (2017) 308.

[93] H. Jóźwiak, F. Thibault, N. Stolarczyk, P. Wcisło, Ab initio line-shape calculations for the S and O branches of H_2 perturbed by He, J. Quant. Spectrosc. Radiat. Transf 219 (2018) 313–322.

[94] J. O. Hirschfelder, C. F. Curtiss, R. B. Bird, Molecular Theory of Gases and Liquids, Wiley, 4th edition, 1967.

[95] G. Kowzan, H. Cybulski, P. Wcisło, M. Słowiński, A. Viel, P. Masłowski, F. Thibault, Subpercent agreement between ab initio and experimental collision-induced line shapes of carbon monoxide perturbed by argon, Phys. Rev. A 102 (2020) 012821.

[96] A. Mantz, F. Thibault, J. Cacheiro, B. Fernandez, T. Pedersen, H. Koch, A. Valentin, C. Claveau, A. Henry, D. Hurtmans, Argon broadening of the ^{13}CO R(0) and R(7) transitions in the fundamental band at temperatures between 80 and 297 K: comparison between experiment and theory, J. Mol. Spectrosc 222 (2003) 131–141.

[97] W. Deng, D. Mondelain, F. Thibault, C. Camy-Peyret, A. W. Mantz, Experimental He-pressure broadening for the R(10) and P(2) lines in the ν_3 band of $^{13}CO_2$, and experimental pressure shifts for R(10) measured at several temperatures between 300K and 100K, J. Mol. Spectrosc 256 (2009) 102–108.